Regional Myocardial Deformation in Adult Patients with Isolated Left Ventricular Non-compaction Cardiomyopathy

Referent: Prof. Dr. med. Frank Weidemann

Koreferent: Prof. Dr. med. Meinrad Beer

Dekan: Prof. Dr. med. Matthias Frosch

Tag der mündlichen Prüfung: 25 February 2011

Die Promovendin ist Ärztin

Contents

Summary

Isolated left ventricular non-compaction cardiomyopathy (LVNC) is a congenital myocardial disease characterized by excessive and prominent trabeculations in the left ventricle with deep intertrabecular recesses. Trabeculation is, however, a non specific finding which is present not only in LVNC but also in other cardiomyopathies like dilated cardiomyopathy (DCM) and even in healthy controls, therefore, differential diagnosis keeps puzzling clinicians. Therefore the present study aimed to comprehensively explore regional myocardial deformation properties in adult patients with isolated LVNC using strain and strain rate imaging derived from tissue Doppler imaging and 2D speckle tracking. It was proposed that the knowledge of deformation properties in LVNC would help to differentiate patients with LVNC and DCM.

A total of 14 patients with LVNC, 15 patients with DCM, and 15 healthy controls were included in this study. The groups were matched for age and gender. Standard 2D echocardiography was performed in all subjects, and tissue Doppler imaging (TDI) of all ventricular walls was acquired using parasternal long axis, apical 4-chamber, 2-chamber, and apical long axis views. Deformation imaging data derived from both TDI and grey scale images were analyzed.

Clinical and standard echocardiographic findings in patients with LVNC and DCM were similar. In patients with LVNC, hypertrabeculation was mostly located in the apical and mid segments of the left ventricle and strikingly more than in patients with DCM. The extent of non-compaction was poorly related to global left ventricular systolic function (LVEF) as well as regional myocardial function assessed by strain rate imaging. Regional myocardial systolic deformation in patients with LVNC was significantly impaired in the left and right ventricles in both longitudinal and radial direction. There was a striking difference on longitudinal myocardial systolic function between LVNC and DCM patients, i.e., an increasing strain and strain rate gradient from apex to base in patients with LVNC, whereas patients with DCM displayed a homogeneously decreased strain and strain rate in all segments. Results derived from 2D speckle tracking method were consistent with those from TDI method. Analysis of myocardial mechanical asynchrony revealed a lack of myocardial contraction synchrony in the LVNC and DCM patients. The time to systolic peak velocity was obviously delayed in these two patient groups. However, the mechanical asynchrony features were similar in patients with LVNC and DCM and could not serve for differential diagnosis.

In conclusion, LVNC and DCM are both cardiomyopathies presenting reduced regional myocardial function and mechanical asynchrony. Nevertheless differential diagnosis can be made by analysis of hypertrabeculation as well as analysis of regional myocardial deformation pattern.

1. Introduction

Isolated left ventricular non-compaction cardiomyopathy (LVNC) is a congenital myocardial disease characterized by excessive prominent trabeculations in the left ventricle (LV) with deep intertrabecular recesses that communicate with left ventricular cavity but not the coronary circulation. Isolated LVNC was unrecognized until 1984 detected by two-dimensional echocardiography [1]. The prevalence of LVNC identified in different echocardiographic studies ranged from 0.01 to 0.24% [2-5]. LVNC is thought to be the consequence of failure in trabecular regression as demonstrated by trabecular meshwork flattening or disappearance. This process should have been completed in the early fetal period in normal population. Genetically, LVNC in adults is often related to an autosomal dominant inheritance instead of infantile cases that were found to be attributed to mutations in the G 4.5 gene located on the X chromosome [6]. Pathological changes of LVNC heart include extensive spongy transformation of the left ventricular myocardium or prominent coarse trabeculations of the ventricular wall and deep recesses of the ventricular cavity. This extensive trabeculations is most frequently found in the left ventricular apex and its adjacent parts of the lateral and inferior wall [7]. Subendocardial fibrosis [8-12], myocardial fibrosis [13,14], myocardial disorganization [15], myocardial hypertrophy and degeneration [16] are also common pathological findings. Natural history studies showed a poor clinical outcome for LVNC patients with impaired left ventricular function. When the late disease stage is present, LVNC leads to premature cardiac death or patients have to undergo cardiac transplantation. Although LVNC is a congenital heart disease, cardiac symptoms are often absent until adulthood leading to a delayed diagnosis. The main clinical manifestations of LVNC include heart failure as a result of systolic and diastolic dysfunction, arrhythmias and thromboembolic events [2,4,5,17,19]. There are no known specific or sensitive clinical features for LVNC. Thus, imaging modalities, e.g. standard echocardiography and cardiac magnetic resonance (CMR), play a fundamental role in the diagnosis of LVNC. Currently, several echocardiographic diagnostic criteria for LVNC are available, mainly based on the size, number and location of trabeculations derived from its distinct morphological entity [4,8,13]. There is no final consensus which criteria are superior, although the ones from Jenni are widely accepted for the definition of LVNC. The original echocardiographic diagnostic criteria described by Jenni [13] are 1) absence of coexisting cardiac abnormalities; 2) two layers structure with thin compacted myocardial band and markedly thick endocardial non-compacted band which consists of prominent trabeculations, the ratio of the non-compacted layer to the compacted layer >2; 3) distribution of the non-compacted myocardium mainly in the apex and the mid of LV inferior and lateral wall; 4) color Doppler evidence of deep perfused intertrabecular recesses. As a consequence

of technology improvement and the increase in disease awareness of LVNC, it has been evidenced that prominent trabeculations are not only presented in LVNC, but also in some individuals with dilated cardiomyopathy (DCM), hypertrophic cardiomyopathy (HCM), hypertensive heart disease or even in a small number of healthy persons [17,20]. Therefore, this arbitrarily results in an over-diagnosis of this disease - even with up-to-date diagnostic criteria, and the differential diagnosis of LVNC continues puzzling clinicians up to the present. This problem is more complicated due to the several proposed diagnostic LVNC criteria. Patient history and standard echocardiographic assessment of HCM and hypertensive heart disease should allow differentiating these diseases from LVNC, but the differentiation between LVNC and DCM remains challenging.

Dilated cardiomyopathy (DCM) is a cardiac disease with multiple potential etiologies, characterized by dilated cardiac (left ventricular) chamber, thinning of ventricular walls and advanced systolic and diastolic dysfunction. DCM shares many clinical and standard echocardiographic features with LVNC [21,22]. It was recently reported that mutated Cypher/ZASP can cause both DCM and LVNC [23]. Thus, it might be difficult in some cases to differentiate LVNC from DCM using presently available criteria.

Strain and strain rate imaging but not standard echocardiography is able to evaluate regional impairment of myocardium by quantitatively analyzing regional myocardial deformation [24-33], which might be helpful to differentiate different cardiomyopathies.

This study used two deformation imaging methods: tissue Doppler imaging (TDI) and 2D speckle tracking imaging (STI). The aim of our study was to comprehensively investigate regional myocardial deformation in adult patients with isolated LVNC and to generate a myocardial deformation model in patients with LVNC. Moreover, we postulated that a special LVNC deformation pattern would help to differentiate this cardiomyopathy from DCM. Another aim of this study was to propose an effective and practicable method performed in echocardiography routine to assess regional myocardial deformation in LVNC.

2. Methods

2.1 Study Population

Between March 2007 and December 2009, a total of 26 consecutive patients with the initial diagnosis of LVNC were screened at the university hospitals of Wuerzburg and Zagreb and 14 patients (8 males, mean age 41± 9 years) with the final diagnosis of LVNC were enrolled in the study and 12 patients were excluded due to uncertain LVNC cardiomyopathy diagnosis. The aim of the study is to observe if there is a typical deformation pattern in LVNC patients. Inclusion criteria for a patient, initially diagnosed as LVNC, to enter the study were: A full available set-up of comprehensive evaluation according to clinical presentation, echocardiography, electrocardiogram and CMR. Moreover, according to actual guideline criteria, three experts in the field of echocardiography and two experienced radiologists had to confirm the LVNC diagnosis independently. Coronary artery disease, cardiac valve disease or other underlying cardiac pathology were excluded by medical history, echocardiography, MRI, exercise test and coronary angiograms. Fifteen age and gender matched patients with confirmed diagnosis of DCM were included in the study (10 males; mean age 49±17 years). Fifteen healthy aged and gender matched volunteers recruited from the local hospital staff (7males, mean age 39±17 years) served as controls. All controls were Caucasian (like all patients), had no history of cardiac or systemic disease or arterial hypertension.

Informed consent was obtained from the patients and healthy subjects.

2.2 Protocol

A complete clinical setup was enrolled. Standard 2D echocardiography was performed in all subjects, and TDI of all ventricular walls was acquired using parasternal long axis, apical 4-chamber, 2-chamber, and apical long axis views. Strain Rate Imaging (SRI) derived from TDI and 2D STI was carried out in different directions of all LV segments.

2.3 Machine Settings and Images Acquisition and Measurement

A commercially available ultrasound scanner (GE Vingmed Vivid 7, Horten, Norway) with a 3.5 MHz transducer was used to collect digital loops in 2-dimensional gray scale imaging, color Doppler flow, pulsed-wave (PW) Doppler, and tissue Doppler imaging. All data measurement and analysis were

conducted by the same observer off-line.

2.4 Standard 2D Echocardiography Measurement

2.4.1 Cardiac Dimensions and LV Mass

Left ventricular end-diastolic (LVEDD) and end-systolic dimensions (LVESD) as well as end-diastolic thickness of the posterior wall (LVPWd) and the septum (IVSd) were measured using standard M-mode echocardiographic methods and parasternal LV long axis images. From parasternal LV long axis images on the level of the left atrium (LA), the end-systolic diameter of the LA was measured. From apical 4-chamber view, the end-diastolic diameter of the right ventricle (RVD) and the end-systolic transversal diameter of the right atrium (RAD) were measured. End-diastolic the maximal thickness of right ventricular free wall (RVd) was measured using the same view. Echocardiography-based left ventricular mass was estimated from M-mode measurements using the Devereux formula.

2.4.2 Global LV Systolic Function

LV ejection fraction (EF) was measured with the biplane Simpson method in apical 4- and 2-chamber views; LV stroke volume (SV), fractional shortening (FS) were assessed by M-Mode method and parasternal LV long axis images. Mitral annular (the septal and lateral wall) displacement and tricuspid plane annular systolic excursion (TAPSE) were measured by M-mode method in apical 4-chamber view.

2.4.3 LV Filling Pattern

Pulsed-wave Doppler was performed in the apical 4-chamber view to obtain mitral inflow velocities in order to evaluate left ventricular filling pattern (early filling (E-wave) and late diastolic filling (A-wave) velocities, the E/A ratio, deceleration time (DT)). Thereafter the cursor of CW Doppler was placed between the LV outflow tract and the anterior tip of the mitral leaflet to simultaneously display the end of ventricular outflow and the onset of mitral inflow to determine the isovolumetric relaxation time (IVRT).

2.4.4 Non- and Compacted Myocardial Measurement

The thickness of non-compacted and compacted myocardial layers was measured at end-systole in all segments (eighteen-segment left ventricular echocardiographic model) using apex 4-, 2-chamber and apical long axis view. The maximal thickness of non-compacted myocardium (NCd) in each segment was measured as an absolute assessment for the local trabeculations extent. Ratio of non-compacted (NC) to compacted (C) layer (NC/C ratio) was calculated as an index to identify hypertrabeculation (figure 1). Segments with NC/C ratio ≥2.0 were defined as hypertrabeculation.
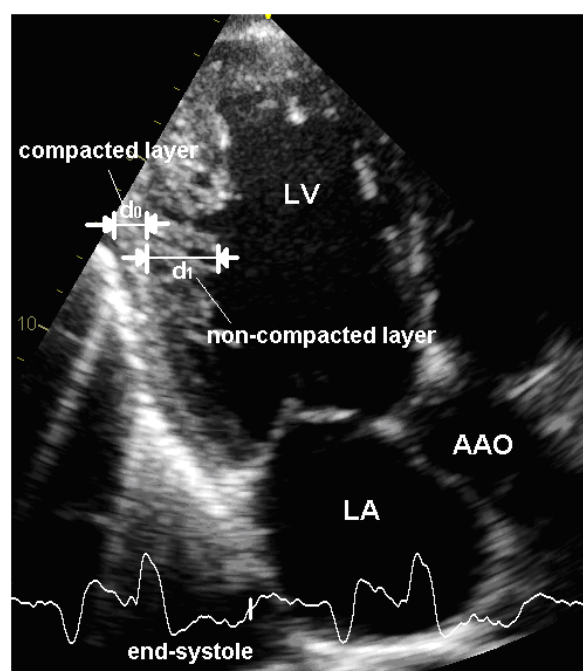
Figure 1: Measurement of non-compacted and compacted myocardium. d_0: thickness of compacted layer; d_1: thickness of non-compacted layer. NCd = d_1; NC/C ratio = d_1/d_0. LV: left ventricle; LA: left atria; AAO: ascending aorta.

2.5 Tissue Doppler Imaging

Tissue Doppler imaging was obtained using left ventricular apical 2-chamber, 4-chamber, and apical long axis view, including septum, lateral wall, inferior wall, anterior wall, posterior wall and anteroseptal wall. TDI of posterior wall using left ventricular parasternal long axis view was obtained to assess the radial myocardial deformation. TDI of the right ventricular free wall was obtained using apical 4-chamber view. Tissue Doppler images views were optimized for pulse repetition frequency, color saturation, sector size and depth, and allowed the highest possible frame rate. Patients were required to hold breath during tissue Doppler images storing. At least three consecutive cardiac cycles

were recorded in a cine loop format and averaged when analyzed.

Tissue Doppler early diastolic mitral annular velocity (e') was obtained in apical 4-chamber view. The sample volume was positioned at or 1 cm within the septal and lateral insertion sites of the mitral leaflets and adjusted as 5-10 mm to cover the longitudinal motion of the mitral annulus in both systole and diastole. E/e' was calculated.

2.6 Strain Rate Imaging Derived from Tissue Doppler Imaging

Strain rate imaging in apical, mid, and basal segments of each wall was analyzed offline using Q-Analysis of the dedicated software (EchoPAC$^{®}$ version 108.1.5 GE ultrasound). The requested criteria for analyzing were that the image quality should be reasonably good and all analyzed myocardial segments should be clearly visible on each frame. In order to maintain the highest possible frame rate (typically, > 140FPS), narrower image sector angle with lower depth was used.

2.6.1 Profiles Acquisition

Strain and strain rate profiles were acquired through post processing offline using dedicated software program. In post processing, eighteen-segment left ventricular echocardiographic mode was used (figure 2). The segments with great angle deviation were excluded from analysis. Region of interest (ROI) was continuously positioned by manual tracking within the wall throughout the cardiac cycle. It should be made sure that the ROI was continuously positioned within the compacted myocardial region instead of non-compacted region. Height of ROI was set to 13 mm in LV and RV longitudinal strain rate analysis. Height of ROI was adjusted according to LVPWd in LV radial strain rate analysis. Width of ROI was set to 1-3 mm. Tilt angle of ROI was as parallel as possible with ultrasound beam. Strain length (offset distance) was usually set to less than 1-2 mm height of ROI. Strain rate profile was averaged over three consecutive cardiac cycles and integrated over time to derive natural strain profiles using end-diastole as the reference point. Aortic valve opening (AVO), aortic valve closure (AVC), mitral valve opening (MVO), and mitral valve closure (MVC) were marked from PW Doppler traces in aortic inflow and mitral inflow respectively to define the isovolumetric contraction time (IVCT), ejection phase, isovolumetric relaxation time and diastolic phase.
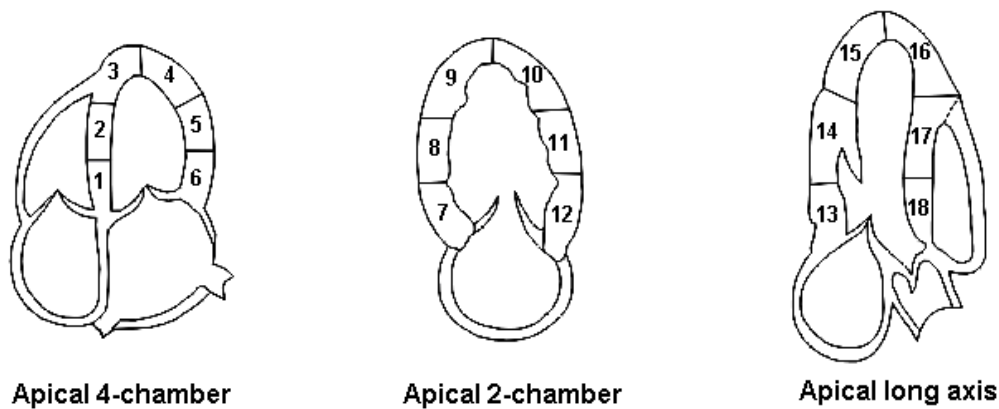
Figure 2: Eighteen-segment left ventricular echocardiographic mode. 1: basal septal wall; 2: mid septal wall; 3: apical septal wall; 4: apical lateral wall; 5: mid lateral wall; 6: basal lateral wall; 7: basal inferior wall; 8: mid inferior wall; 9: apical inferior wall; 10: apical anterior wall; 11: mid anterior wall; 12: basal anterior wall; 13: basal posterior wall; 14: mid posterior wall; 15: apical posterior wall; 16: apical anteroseptal wall; 17: mid anteroseptal wall; 18: basal anteroseptal wall.

2.6.2 Parameters acquisition

The following strain rate (SR) data was extracted. Strain and strain rate data measurement are shown in figure 3a.

- Systolic peak strain rate (SR_S).
- Peak SR in isovolumetric contraction time (SR_IVCT).
- Peak SR in isovolumetric relaxation time (SR_IVRT).
- Early diastolic peak strain rate (SR_E).
- Late diastolic peak strain rate (SR_A).

  Strain (S) data comprise the parameters as showed below (figure 3b).

- Maximal strain in one cardiac cycle (S_max_cyc), measured from the absolute maximum to minimal strain value.

- Maximal strain in ejection phase (S_max_sys), measured from AVO to the maximum during ejection phase.

- Strain at the end of ejection period (S_end_sys), measured from AVO to AVC.

- Post systolic shortening (PSS), measured from AVC to the shortening/lengthening cross point.

  Pathological post systolic shortening (PSS) was defined according to Jens-Uwe Voigt's criteria [34]: PSS exceeding 20% of total strain in one cardiac cycle (S_max_cyc) or shortening duration more than 90 ms from AVC to PSS peak.

a)
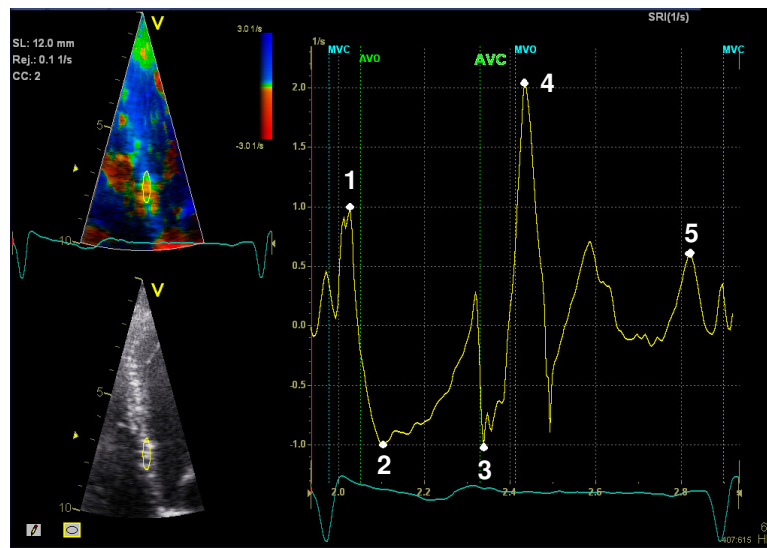
b)
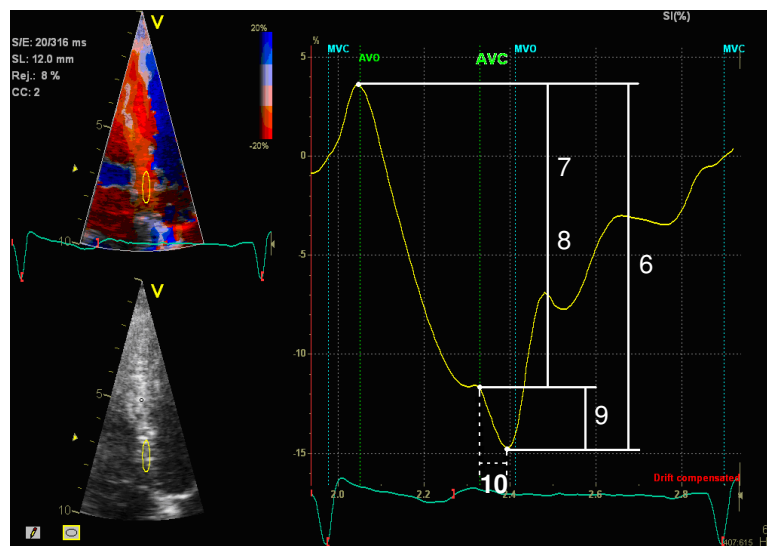
Figure 3a+b: Typical strain rate and strain profiles of a healthy subject derived from tissue Doppler imaging and explanation of measurements. a) 1: systolic peak strain rate (SR_S); 2: peak strain rate in isovolumetric contraction time (SR_IVCT); 3: peak strain rate in isovolumetric relaxation time (SR_IVRT); 4: early diastolic strain rate (SR_E); 5: late diastolic strain rate (SR_A); 6: maximal strain in one cardiac cycle (S_max_cyc); b) 7: maximal strain in ejection phase (S_max_sys); 8: end systolic strain (S_end_sys); 9: post systolic shortening (PSS); 10: shortening duration of PSS.

2.7 Strain Rate Imaging Derived from 2D Speckle Tracking

2D speckle tracking imaging, obtained by 2D gray scale using standard 2-, 4-chamber views, was investigated in patients with LVNC and DCM. Septum, lateral, inferior and anterior wall were involved in this part.

2.7.1 Profiles Acquisition

The 2D grey scale frame rate was set in between 40 to 80 frames per second. It was made sure that the entire ventricular wall was clearly visible. The scanner was configured to store heart cycles with 100 milliseconds before and after the R-wave. The ROI was created by manual outlining of the endocardial border in a single wall and had to cover the entire region to be analyzed. Of note, the ROI only covered the compacted myocardial region in patients with LVNC. Thereafter, the processing screen was displayed showing the ROI divided into segments automatically. The tracking quality for each segment was automatically evaluated and summarized in the tracking table. If necessary the tracking had to be visually checked and adjusted. The trace analysis was automatically displayed after validating the tracking. The strain profile of one cardiac cycle for three segment levels (apical, mid and basal segment) was displayed by the software simultaneously as shown in figure 4.

a)

b)
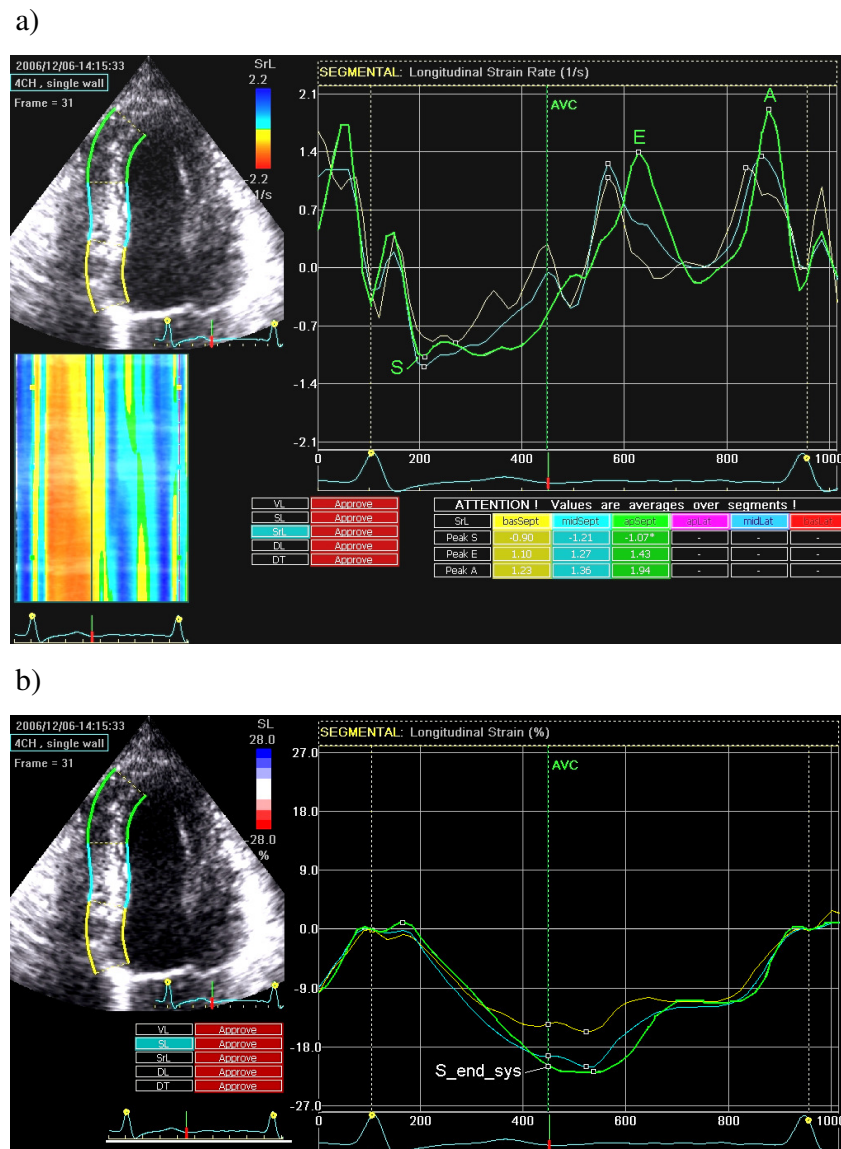
Figure 4a+b: An example of strain rate (a) and strain (b) profiles derived from 2D speckle tracking imaging in the septum of a normal subject. The ROI was created by manual outlining of the endocardial border in septum. Yellow, blue and green sections respectively represent the basal, mid and apical segment. a) Longitudinal strain rate curve, Peak S: systolic strain rate; Peak E: early diastolic strain rate; Peak A: late diastolic strain rate. b) Longitudinal strain curve, S_end_sys: end systolic strain.

2.7.2 Parameters Measurement

Using 2D speckle tracking method, end systolic strain (S_end_sys) for all segments in each wall was measured. Global longitudinal end systolic strain for each entire wall was obtained by averaging strain values for the LV three segment levels, as shown in figure 5.

a)

b)
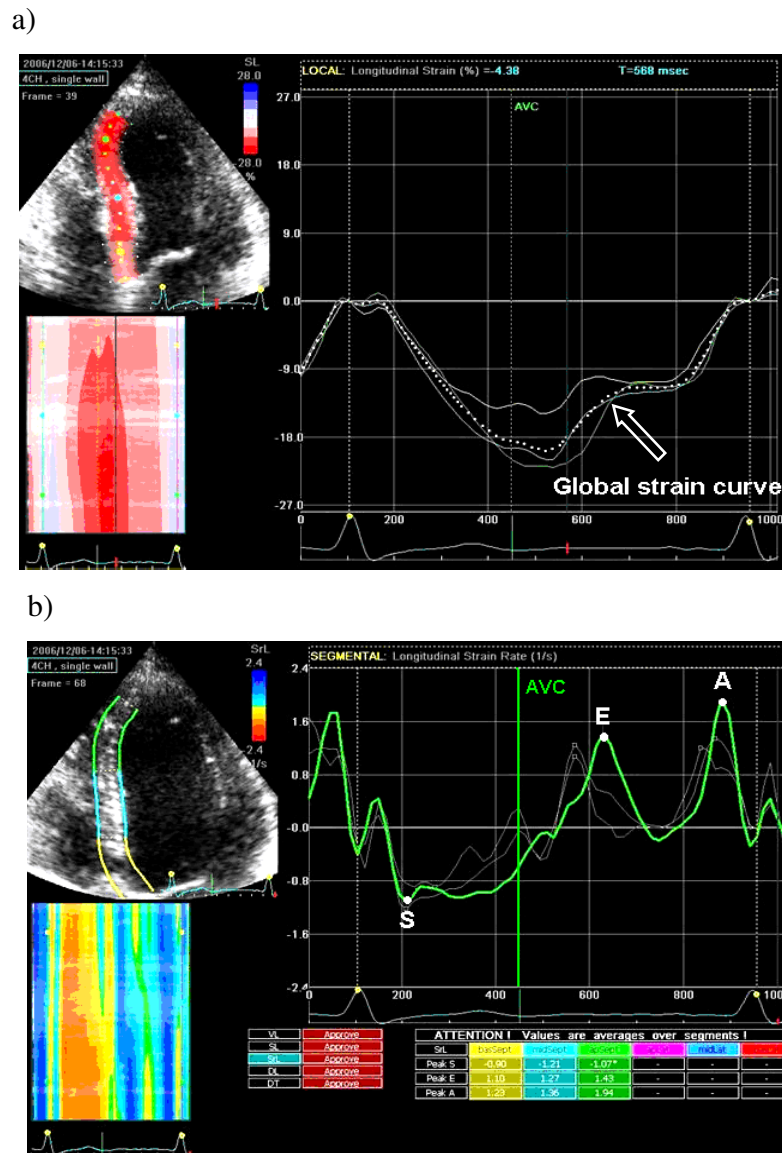
Figure 5 a+b: a) shows a global strain curve of the septum (dashed curve); b) shows a strain rate curve in apical septum (green curve). Peak S: systolic peak strain rate; Peak E: early diastolic peak strain rate; Peak A: late diastolic peak strain rate.

2.8 LV Mechanical Asynchrony

2.8.1 Standard Echocardiography

The septal-to-posterior-wall motion delay (SPWMD) by M-mode in LV parasternal long axis view at mitral chordae tendineae level was calculated (figure 6a), to provide information about intraventricular mechanical asynchrony.

Aortic pre-ejection interval (APEI, from QRS wave in the ECG to the beginning of aortic flow derived by pulsed-wave Doppler) was calculated. (figure 6b).

a)   b)
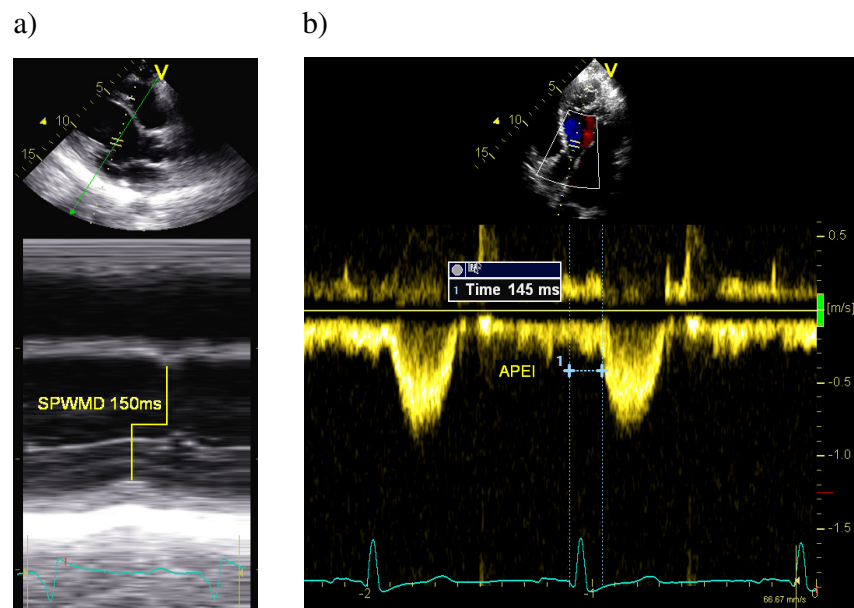
Figure 6: a) M-mode (LV parasternal long axis view) at mitral chordae tendineae level of the left ventricle for measuring the septal-posterior-wall motion delay (SPWMD). The SPWMD is approximately 150ms in this LVNC patient. **b)** Aortic pre-ejection interval (APEI) is measured from QRS wave to the beginning of aortic flow derived by pulsed-wave Doppler (APEI: 145ms).

2.8.2 Tissue Velocity Imaging

Tissue velocity-time profiles of four segments (basal and mid septum, basal and mid lateral wall) were obtained in all subjects. The time to systolic peak velocity (T_sys) was measured and the difference of time to peak velocity in ejection phase within different segments as well as different LV walls was calculated (figure 7).
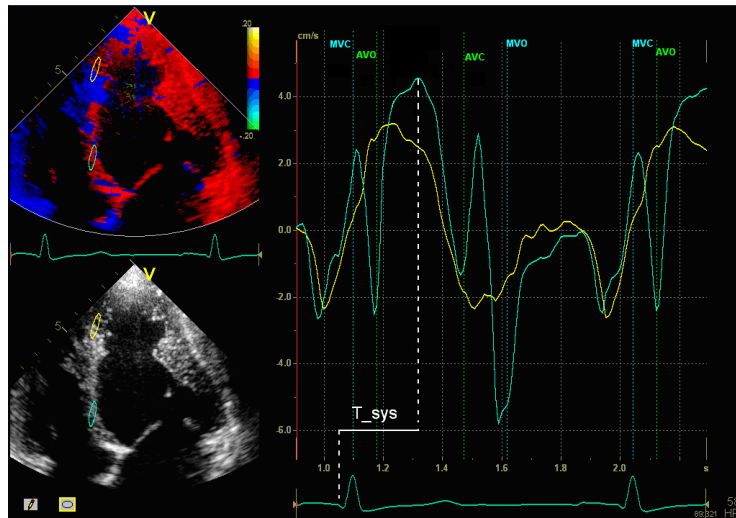
Figure 7: Measurement of T_sys by tissue velocity-time profile derived from tissue Doppler imaging. The time to systolic peak velocity (T_sys) is measured from QRS wave to the peak systolic velocity. Regions of interest (ROI) are positioned at the basal septum (blue) and the apical septum (yellow) respectively.

2.8.3 Speckle Tracking Imaging

The time from QRS wave to the compression and expansion crossover (T_{CEC}) by strain profiles derived from 2D STI was calculated in three segment levels of the septum and lateral walls (figure 8). The maximal difference of T_{CEC} (max-Δ T_{CEC}) among six segments was also calculated.
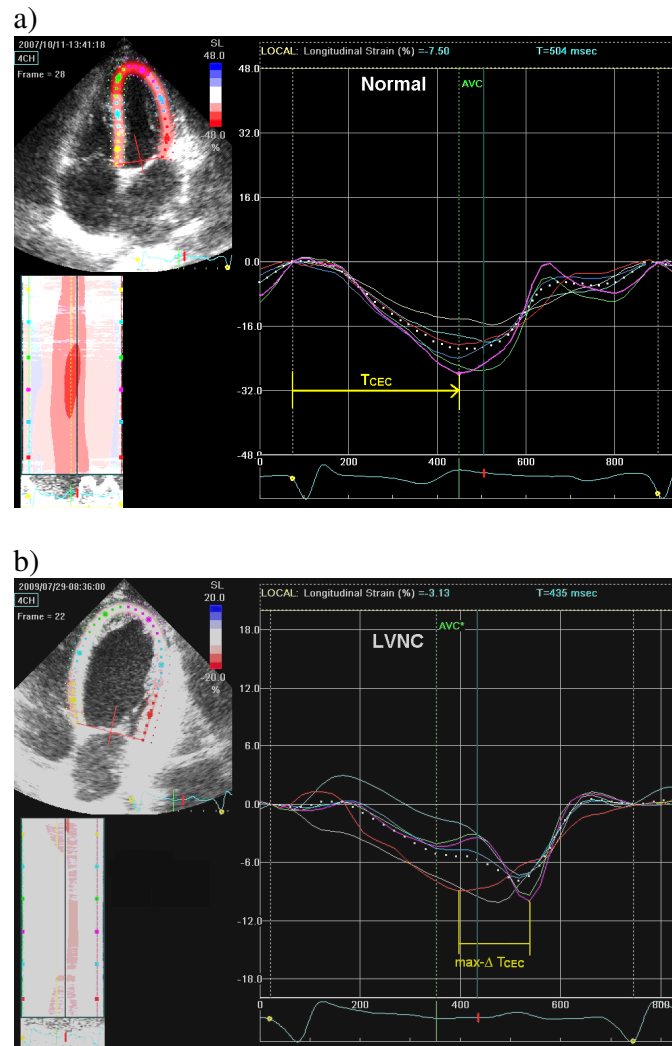
Figure 8 a+b: Measurement of the T_{CEC} and max-ΔT_{CEC} by strain profile derived from 2D speckle tracking imaging. a) The time from the beginning of QRS wave to the compression and expansion crossover (T_{CEC}) is measured from QRS wave to the shortening/lengthening cross point in one cardiac cycle. b) Max-ΔT_{CEC} is the maximal time difference of T_{CEC} derived from 6 segments.

2.9 Statistical Analysis

Data are presented as mean ± standard deviation or 95% confidence interval. Differences among different groups and among different segments were compared using an unpaired Student t-test, one-way or two-way ANONA, as appropriate after performing Normality Test and Equal Variance Test. All pairwise multiple comparison procedures used Tukey's Test if Normality Test and Equal Variance Test were passed. If not Dunn's Method, Student-Newman-Keuls Method, or Mann-Whitney Rank Sum Test was used. Differences of the proportions within the two groups were compared using z-test. Linear regression analysis was used to reveal the correlation between deformation parameters and NC/C ratio. A p value < 0.05 was considered statistically significant. Statistical analysis was performed using statistic software SigmaStat 2.0.

3. Results

3.1 Clinical Data and Standard Echocardiography Findings

Clinical data of all subjects are listed in table 1. Standard echocardiography findings are shown in table 2.

In this cohort, heart failure symptoms are presented in 57% LVNC patients and 53% DCM patients. Abnormalities of ECG were common in LVNC and DCM patients (table 2). Systemic embolization was seen in one LVNC patient and LV thrombus was identified in another LVNC patient. There was no family history in any LVNC patient.

Left atrial and ventricular enlargements were evidenced by standard echocardiography in both LVNC and DCM patients, with similar dimensions. Right atrial and ventricular cavities were similar between control and patient groups. RV free wall thickness was thicker in DCM group than in control group (p=0.009), and systolic pulmonary artery pressure was significant higher in DCM patients than in LVNC patients and control subjects (p<0.001). Left ventricular mass was similar between the two patient groups but significantly higher than in control group (p<0.001 respectively).

Global left ventricular systolic function determined by FS and EF was significantly reduced in both LVNC and DCM groups. Likewise, mitral and tricuspid annular displacements were significantly decreased in LVNC and DCM groups. Lateral annular displacement was significantly higher than septal annular displacement in LVNC group, and this difference was not observed in DCM group. Diastolic function was reduced in both LVNC and DCM groups, advanced diastolic dysfunction (pseudonormal relaxation and restrictive filling pattern) were shown in 9 LVNC patients (69.2%) and in 10 DCM patients (66.7%). E/e' was significantly higher in DCM group than in controls and LVNC patients.

Mitral regurgitation was documented in the majority of patients with LVNC (92.3%, 10 mild and 2 moderate) and DCM (86.7%, 10 mild and 3 moderate).

Table 1: Clinical characteristics of controls and patient groups

	Control n = 15	LVNC n = 14	DCM n = 15
General data			
Age, y	39 ± 17	41 ± 9	49 ± 17
Gender, M	7 (47%)	8 (57%)	10 (67%)
NYHA class	1	1.8 ± 0.5	2.3 ± 1.1
Heart rate, bpm	74 ± 21	72 ± 12	87 ± 23
Systolic BP, mmHg	120 ± 10	117 ± 9	127 ± 21
Diastolic BP, mmHg	80 ± 8	73 ± 9	81 ± 18
Familial occurrence	-	0	1
EKG			
Atrial fibrillation	0	1 (7%)	0
Left bundle branch block	0	5 (36%)	5(33%)
Right bundle branch block	0	2 (14%)	0
Atrioventricular block (I°)	0	2 (14%)	1 (7%)
Ventricular arrhythmias	0	6 (43%)	1 (7%)
Repolarization abnormality	0	4 (29%)	6(40%)
Clinical symptoms			
Heart failure symptoms	0	8 (57%)	8(53%)
Systemic embolic events	0	1 (7%)	0
Ventricular thrombi	0	1 (7%)	0
Death	0	0	0
Heart transplantation	0	0	0

LVNC: left ventricular non-compaction; DCM: dilated cardiomyopathy

Table 2: Standard echocardiography data of control and patient groups

	Control n = 15	LVNC n = 14	DCM n = 15
Cardiac dimensions			
LAD, mm	32.3 ± 3.2	45.8 ± 8.0*	44.7 ± 6.4*
LVEDD, mm	49.0 ± 2.8	62.5 ± 6.4*	67.5 ± 8.6*
IVSd, mm	8.1 ± 1.6	9.2 ± 1.5	8.2 ± 1.7
LVPWd, mm	8.1 ± 1.5	9.6 ± 1.7	9.1 ± 2.0
RVd, mm	4.4 ± 0.5	4.6 ± 1.1	5.7 ± 1.4*
RVD, mm	33.5 ± 4.9	36.6 ± 5.4	38.5 ± 7.7
RAD, mm	37.8 ± 5.3	41.6 ± 6.8	43.8 ± 11.4
LVM, g	135 ± 36	246 ± 48*	259 ± 81*
LV systolic function			
SV, ml	75.9 ± 14.7	67.8 ± 35.2	70.2 ± 25.0
FS, %	36.8 ± 5.0	15.9 ± 6.2*	15.0 ± 5.9*
EF, %	64.1 ± 5.3	30.8 ± 9.4*	30.1 ± 9.9*
Septal_MAD, mm	13.7±2.1	5.5±1.9*	5.9±3.2*
Lateral_MAD, mm	14.5±2.2	7.9±3.3*	7.1±2.9*
TAPSE, mm	23.3±4.0	15.5±3.7* ‡	17.7±3.8*
LV filling pattern			
Normal filling	14	1	0
Abnormal relaxation	1	4	5
Pseudonormal relaxation	0	4	3
Restrictive	0	5	7
E/A	1.44 ± 0.29	1.57 ± 1.18	1.69 ± 1.02
E/e'	8.0 ± 2.8	13.1 ± 5.5	20.5 ± 8.1*†
DT, ms	190 ± 37	147 ± 55	152 ± 58
IVRT, ms	91 ± 21	84 ± 33	81 ± 33
Mitral regurgitation	7 (47%)	12 (86%)	13 (87%)
Aortic regurgitation	1 (7%)	1 (7%)	4 (27%)
SPAP, mmHg	17.7 ± 9.8	24.9 ± 9.9	37.5 ± 14.9*†

LV: left ventricle; LAD: end-systolic left atrial diameter; LVEDD: left ventricle end-diastolic dimension; IVSd: end-diastolic interventricular septum thickness; LVPWd: end-diastolic left ventricular posterior wall thickness; RVd: end-diastolic right ventricular free wall thickness; RVD: end-diastolic right ventricular dimension; RAD: end-systolic right atrial diameter; LVM: left ventricular mass; SV: LV stroke volume; EF: LV ejection fraction; FS: LV fractional shortening; MAD: mitral annular displacement; TAPSE: tricuspid annular plane systolic excursion; E/A: early diastolic filling velocity (E) to late diastolic filling velocity (A) ratio; E/e': mitral inflow E velocity to tissue Doppler e' ratio; DT: deceleration time of early filling; IVRT: isovolumetric relaxation time; SPAP: systolic pulmonary artery pressure. * $p<0.05$ vs. Control   † $p<0.05$ vs. LVNC   ‡ $p<0.05$ vs. Septal mitral annular displacement

3.2 Left Ventricular Trabeculations

3.2.1 Number and Location of Trabeculations in LVNC and DCM

Trabeculations were present in 134 out of 252 (53.2%) segments in patients with LVNC and in 50 out of 270 segments (18.5%) in patients with DCM (p<0.05). The majority (99.3%) of trabeculations in LVNC patients was located in apical and mid segments (81 apical, 52 mid, 1 basal). The average non-compacted myocardial thickness in apical, mid and basal segments of patients with LVNC derived from 18 segments is shown in figure 9. In DCM group, the majority of trabeculations (92%) was located in apical segments (46 apical, 4 mid).

The mean of NC/C ratio in LVNC patients was significantly higher than those in DCM patients (2.1 ± 0.8 vs. 1.4 ± 0.5, p<0.05).

The distribution of trabeculations and hypertrabeculation in different LV walls of patients with LVNC and DCM is displayed in figure 10. As shown in figure 10b, hypertrabeculation (NC/C ratio ≥2.0) was presented in 79 out of 252 segments (31.3%) in LVNC group (60 apical, 19 mid) and only in 9 segments out of 270 segments (3.3%, p<0.001 vs. LVNC) in DCM group (8 apical, 1 mid). Hypertrabeculation was not found in mid septum segments of patients with LVNC in this cohort.
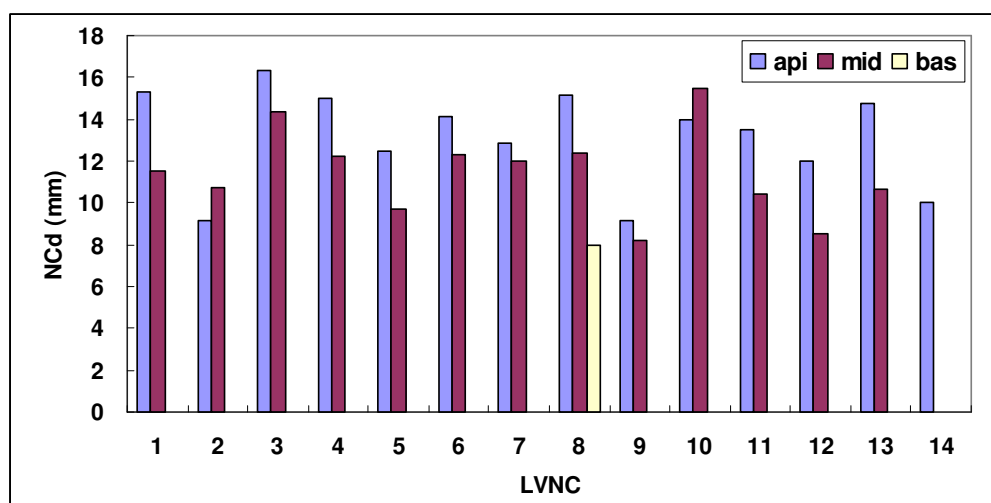
Figure 9: The average non-compacted myocardium thickness in apical, mid and basal segments of individual LVNC patient derived from 18 segments. Note that trabeculations in LVNC was mainly present in apical and mid segments and trabeculation was seen only in one basal segment.

a)

b)
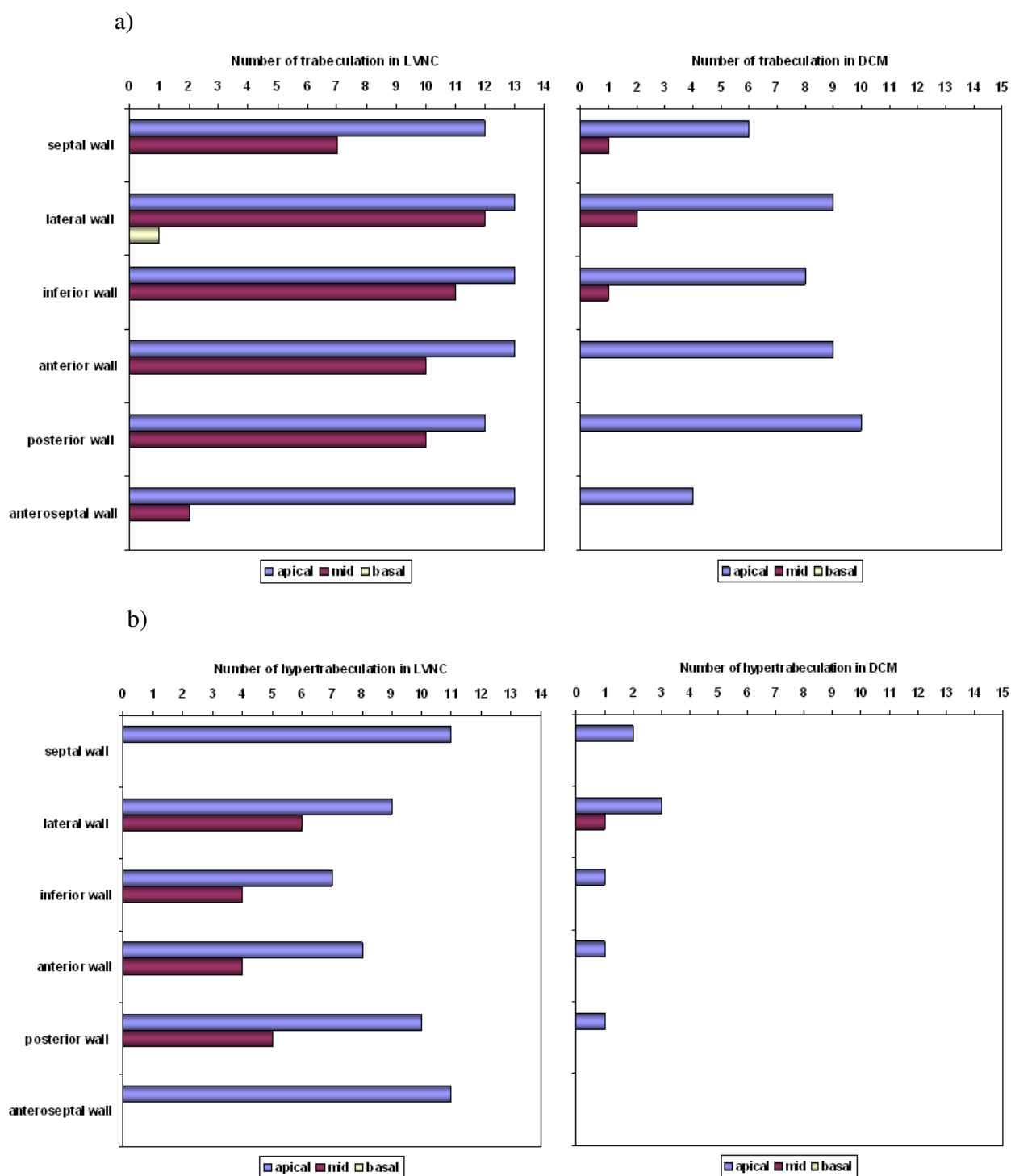
Figure 10a+b: Number and location of trabeculations and hypertrabeculation in six left ventricular walls of LVNC and DCM groups. a) the distribution of trabeculations; b) the distribution of hypertrabeculation.

3.2.2 Trabeculations and Global / Regional LV Myocardial Function

3.2.2.1 Trabeculations and Global Systolic Function

As shown in figures 11 to 13, there was no linear correlation between maximal NC/C ratio and left ventricular ejection fraction. Septal and lateral mitral annular displacement, representing longitudinal systolic function, was also not related to the maximal NC/C ratio.
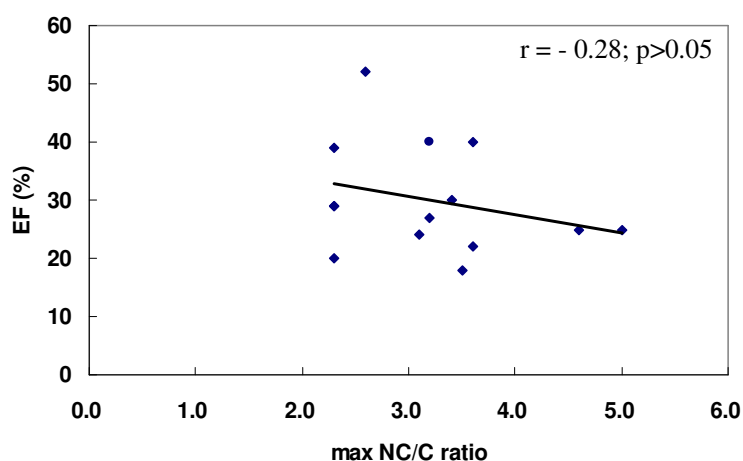
Figure 11: Scatter plot and Pearson's correlation coefficient for left ventricular ejection fraction (EF) and maximal ratio of non-compacted to compacted myocardium (max NC/C ratio). There was no significant correlation between EF and max NC/C ratio.
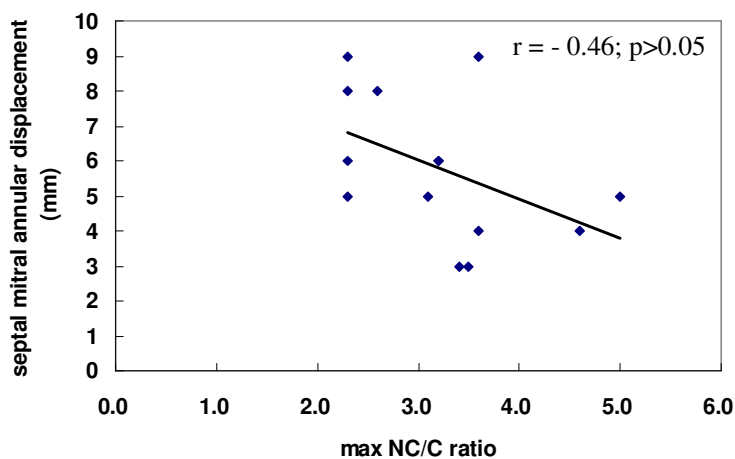
Figure 12: Scatter plot and Pearson's correlation coefficient for septal mitral annular displacement and max NC/C ratio. There was no significant correlation between septal mitral annular displacement and max NC/C ratio.
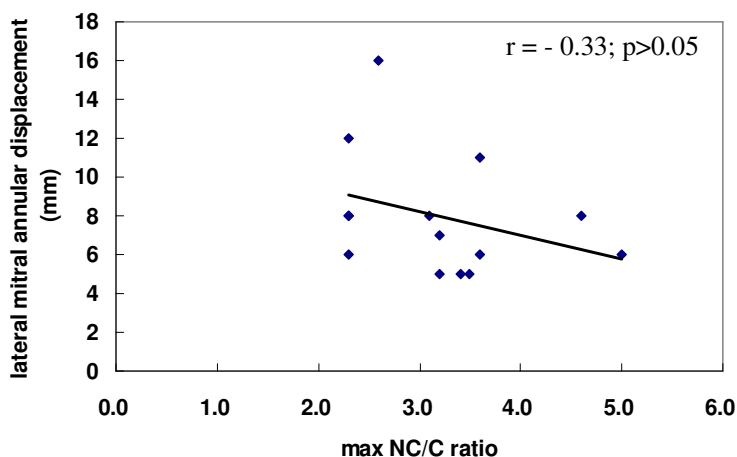
Figure 13: Scatter plot and Pearson's correlation coefficient for lateral mitral annular displacement and max NC/C ratio. There was no significant correlation between lateral mitral annular displacement and max NC/C ratio.

3.2.2.2 Trabeculations and Regional Myocardial Function

Regional myocardial systolic deformation was analyzed on 204 segments in LVNC and 234 in DCM groups including 117 segments with trabeculations (NCd > 0) in LVNC and 46 segments with trabeculations in DCM as well as 87 segments without trabeculations (NCd = 0) in LVNC and 188 segments without trabeculations in DCM.

Figure 14 showed that regional myocardial systolic deformation (SR_S, S_end_sys) was significantly lower in segments with trabeculations than without trabeculations in LVNC group (Mann-Whitney Rank Sum Test, p<0.001). However, no remarkable correlation was seen between the degree of non-compaction (neither NCd nor NC/C ratio) and the regional myocardial deformation indices (figure 15, 16). Regional myocardial deformation indices were similar in segments with and without trabeculations in DCM group.
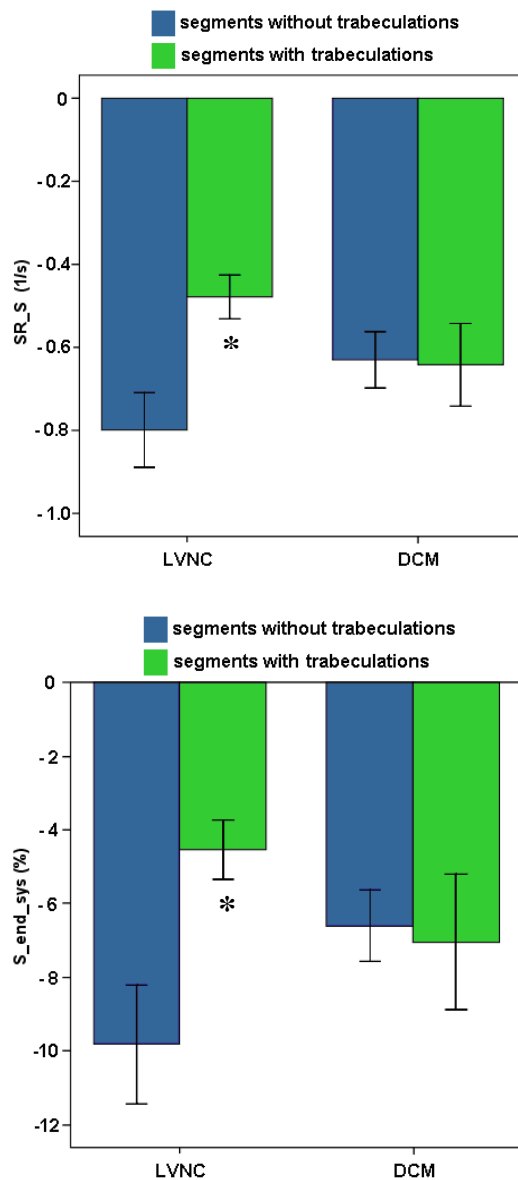
Figure 14: Comparison of myocardial deformation data (mean and 95% CI) between segments with and without trabeculations in LVNC and DCM groups. SR_S: systolic strain rate; S_end_sys: end systolic strain.

* p<0.05 vs. segments without trabeculations
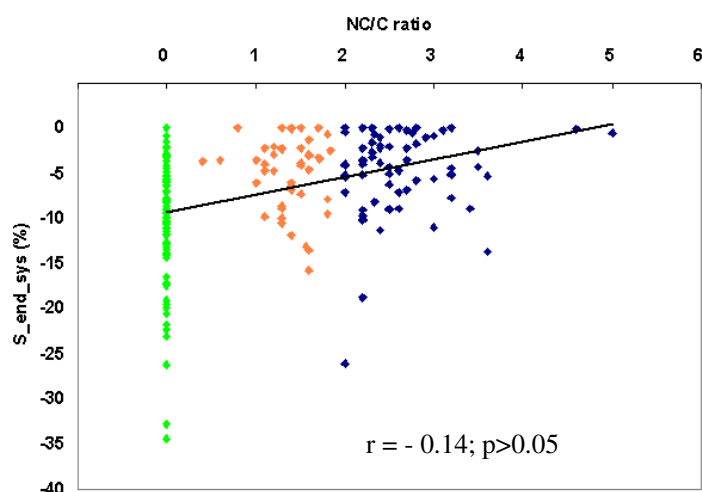
Figure 15: Scatter plot for NC/C ratio and end systolic strain in LVNC group. S_end_sys: end systolic strain; NC/C ratio: the ratio of non-compacted to compacted layer. Green points represent the segments without trabeculations (NC/C ratio= 0), orange points represent the ones with mild non-compaction (0 < NC/C ratio < 2); blue points represent the ones with prominent non-compaction (NC/C ratio ≥2.0).
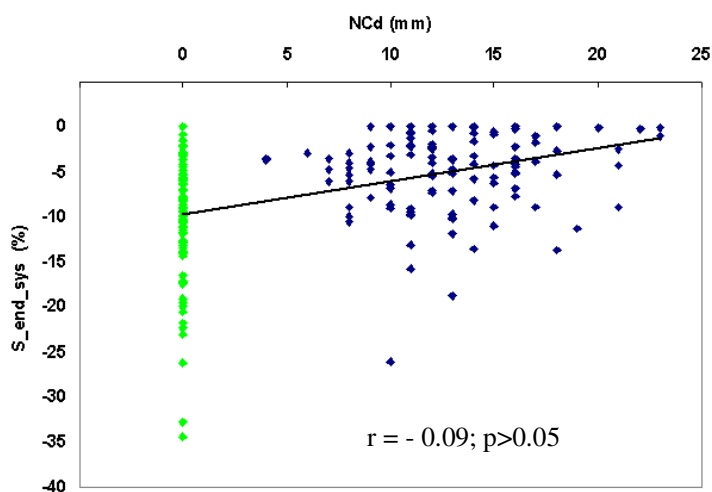
Figure 16: Scatter plot for NCd and end systolic strain during ejection phase in LVNC group. S_end_sys: end systolic strain; NCd: the maximal thickness of non-compacted myocardium in each myocardial segment. Blue and green points respectively represent the segments with and without trabeculations.

3.3 Regional Myocardial Deformation

3.3.1 Regional Myocardial Deformation in Six Left Ventricular Walls

Overall end systolic strain in all left ventricular walls and right ventricular free wall was investigated by tracking a single wall using 2D speckle tracking. Overall end systolic strain in six left ventricular walls between patient groups and controls are displayed in figure 17. Longitudinal systolic deformation in all six LV walls was significantly reduced compared controls.
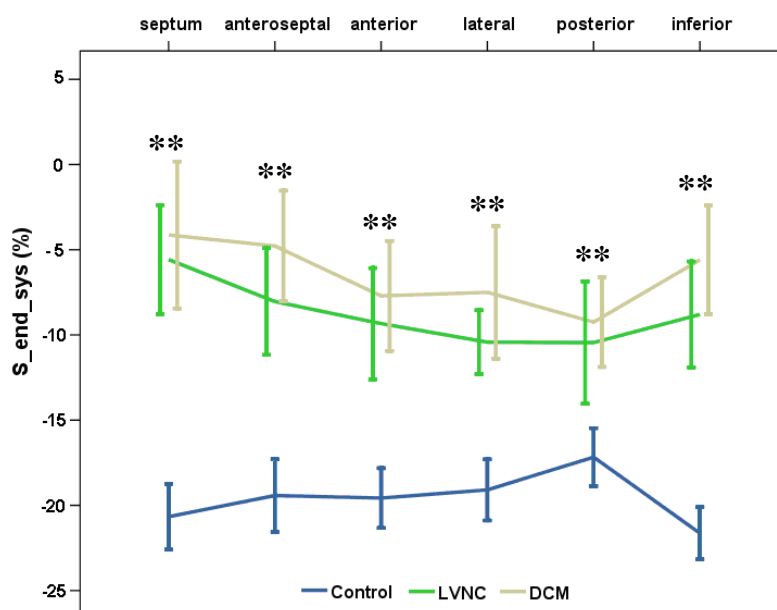
Figure 17: Comparison of left ventricular longitudinal end systolic strain ((mean and 95% CI) in six left ventricular walls between control and patient groups. Note that myocardium longitudinal shortening in all left ventricular walls of LVNC and DCM group was significantly reduced compared to controls. No difference of longitudinal shortening was observed between LVNC and DCM patients in all left ventricular walls.

* $p<0.05$ vs. Control

As shown in figure 18, myocardium systolic radial thickening in basal posterior wall of LVNC and DCM group was significantly lower than that of controls. There was no significant difference between LVNC and DCM group.

Longitudinal end systolic strain in right ventricular free wall was significantly reduced in patients with LVNC and DCM as compared with controls. Likewise, there was no significant difference between LVNC and DCM group (figure 19).
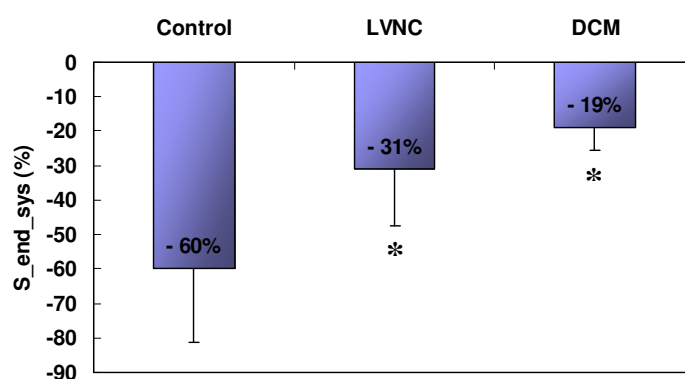
Figure 18: Comparison of radial end systolic strain (mean and 95% CI) in basal posterior wall among controls, LVNC and DCM groups. S_end_sys: end systolic strain.
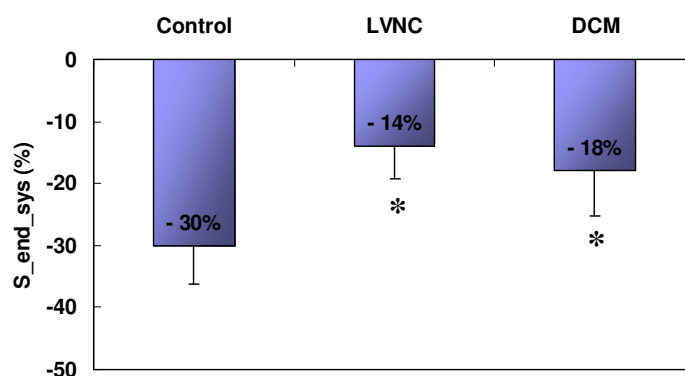
* p<0.05 vs. Control

Figure 19: Comparison of longitudinal end systolic strain (mean and 95% CI) in right ventricular free wall among the different groups. S_end_sys: end systolic strain.

* p<0.05 vs. Control

3.3.2 Regional Myocardial Deformation in Apical, Mid and Basal Levels

As listed in table 3, SR_S and S_end_sys in apical, mid and basal levels of the same ventricular wall were significantly reduced in both LVNC and DCM groups compared with controls, analyzed by TDI. As compared for different levels of the same ventricular wall, SR_S and S_end_sys in basal segments were markedly higher than that in apical and mid segments in patients with LVNC while there were no significant differences among three levels in DCM group. SR_S and S_end_sys in basal segments were significantly higher in LVNC group than those in DCM group.

As shown in figure 20, an increasing deformation gradient from apex to base was documented in all left ventricular walls except anteroseptal wall in LVNC patients. Significant difference of S_end_sys between basal and apical segments was found in lateral, inferior, anterior and posterior walls. End systolic longitudinal shortening in DCM was significantly reduced in all six left ventricular walls and the pattern of increasing gradient from apex to base was not shown in patients with DCM. Figure 21 and 22 show typical strain rate profiles and strain profiles from tissue Doppler imaging in lateral wall of a normal subject, a patient with LVNC and a patient with DCM.

Table 3: LV systolic strain rate (SR_S) and end systolic strain (S_end_sys) at apical, mid and basal segments in controls, LVNC and DCM groups using tissue Doppler imaging

		Control	LVNC	DCM
		n = 15	n = 14	n = 15
Apical	SR_S (1/s)	-1.33 ± 0.49	-0.48 ± 0.37*	-0.59 ± 0.38*
	S_end_sys (%)	-18.05 ± 6.06	-5.22 ± 5.11*	-6.80 ± 6.33*
Mid	SR_S (1/s)	-1.28 ± 0.30	-0.55 ± 0.31*	-0.63 ± 0.47*
	S_end_sys (%)	-17.62 ± 4.87	-5.83 ± 4.52*	-6.06 ± 5.44*
Basal	SR_S (1/s)	-1.22 ± 0.35	-0.81 ±0.41*‡§	-0.59 ± 0.38*†
	S_end_sys (%)	-15.45 ± 5.18‡§	-9.80 ± 7.05*‡§	-5.98 ±5.89*†

* p<0.05 vs. Control   † p<0.05 vs. LVNC   ‡ p<0.05 vs. Apical   § p<0.05 vs. Mid
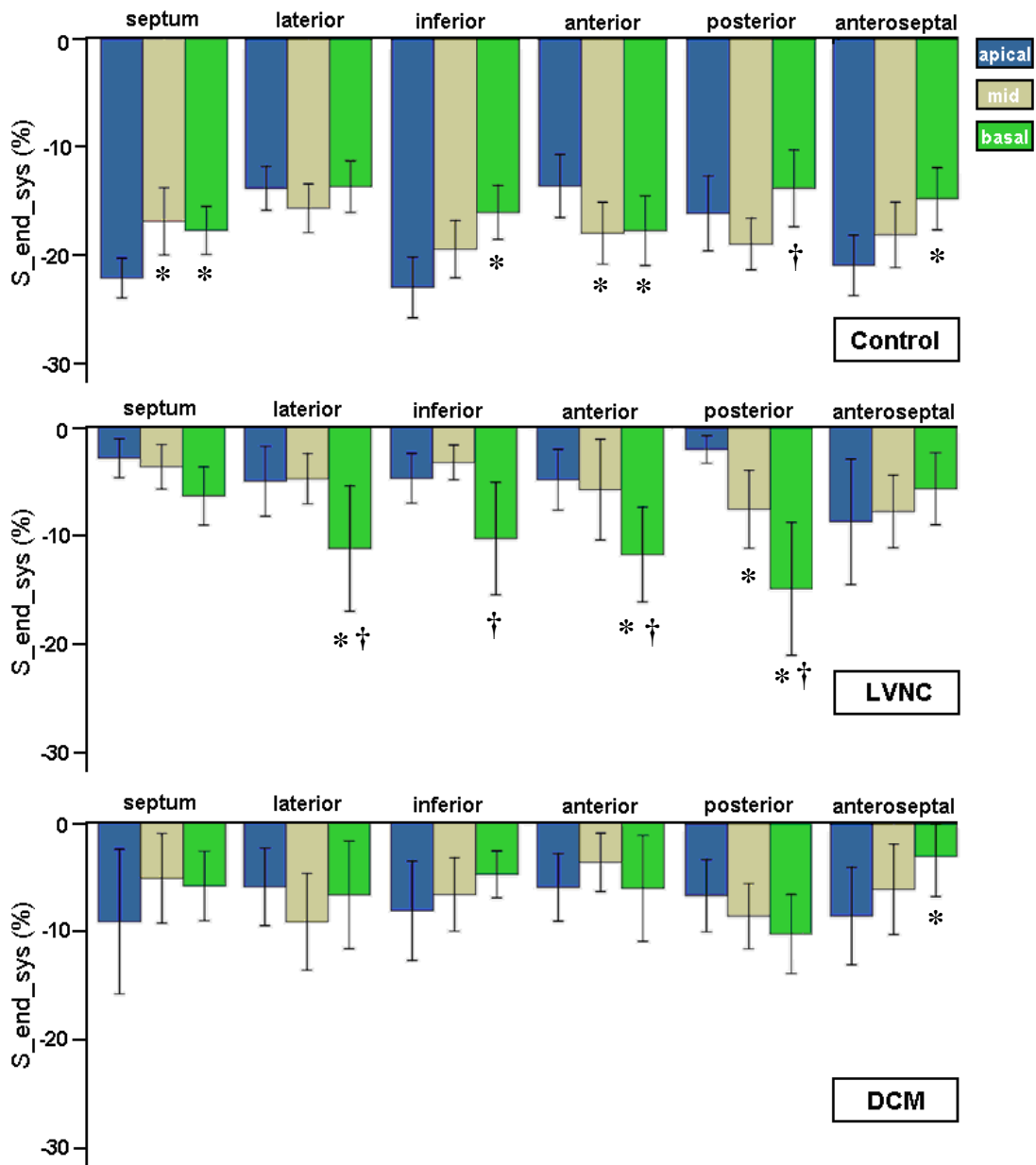
Figure 20: End systolic strain (mean and 95% CI) by tissue Doppler imaging among different segment levels of six LV walls among controls, LVNC and DCM. .

* $p<0.05$ vs. apical   † $p<0.05$ vs. mid
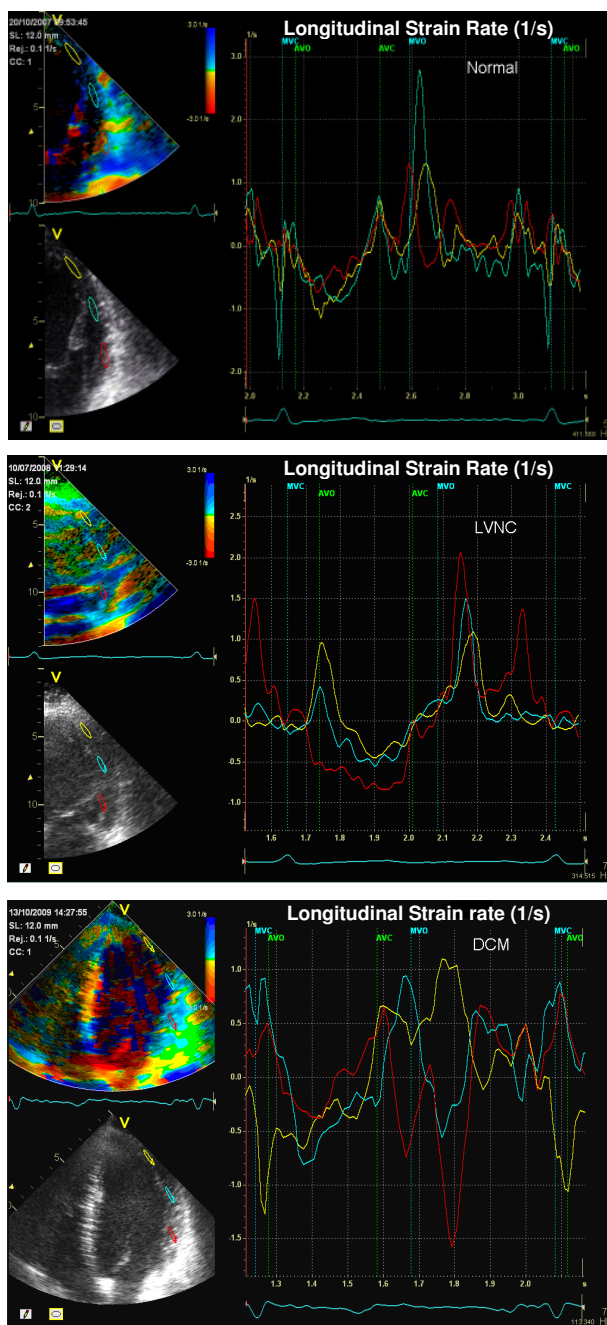
Figure 21: Strain rate profiles in the lateral wall of a normal (above), a LVNC (middle) patient and a DCM (below) patient, using tissue Doppler imaging. Yellow, blue and red curves respectively represent the strain rate curves in the apical, mid and basal segments. Note that systolic strain rate in the apical lateral wall of LVNC is markedly reduced compared with the basal and mid segments, while conversely in DCM and normal subject the lowest value present at the basal segment.
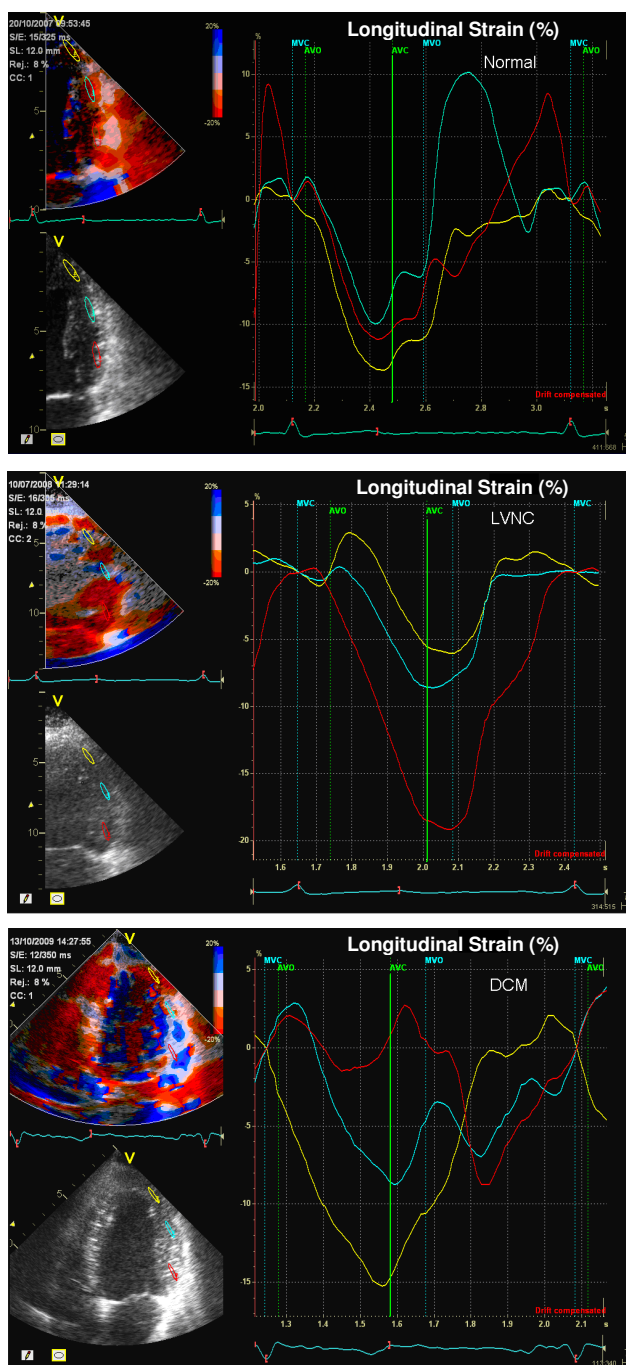
Figure 22: Strain profiles from TDI in three segment levels of lateral wall in the same patients as in figure 21.
Yellow, blue and red curves respectively represent the strain curves in the apical, mid and basal segments. Note similar findings of a decreased strain in the apical segment compared with the strain in the mid and basal segments in LVNC. An increasing gradient in end systolic strain is present in LVNC.

3.4 Shape Features of Strain and Strain Rate Profiles

Strain rate profiles were investigated in apical and basal segments of septum and lateral wall of LVNC, DCM, and control groups. A typical strain rate profile from a normal subject was shown in figure 23. The strain rate and strain profiles in the apical septum of a patient with LVNC were shown in figure 24. In this patient, the peak in ejection phase was significantly reduced and a higher and widen positive peak in IVCT as well as a larger negative peak in IVRT could be evidenced (figure 24). In general, this distinct profile occurred more frequently in LVNC group than in control group (p=0.003) and in DCM group (p=0.003). Moreover this pattern was more frequent in septal walls than in lateral walls of patients with LVNC (p=0.001, table 5). In control group, no apical segments displayed this distinct curve, whereas 37.5% apical segments in LVNC group and 23.3% in DCM presented this kind of curve (table 4).

Table 4: The incidence of the characteristic SR profile in control, LVNC, and DCM groups

	Control (n =60)	LVNC (n = 48)	DCM (n = 60)
Sum, n (%)	10 (16.7)	22(45.8) *	18 (30.0)
Septum, n (%)	8 (26.7)	17 (70.8) *	8 (26.7) †
Lateral wall, n (%)	2 (15.0)	5 (20.8) ‡	10 (33.3)
Apical segments, n (%)	0	9 (37.5)	7 (23.3)
Basal segments, n (%)	10 (33.3)	13 (54.2)	11 (36.7)

* p<0.05 vs. Control   † p<0.05 vs. LVNC   ‡ p<0.05 vs. Septum
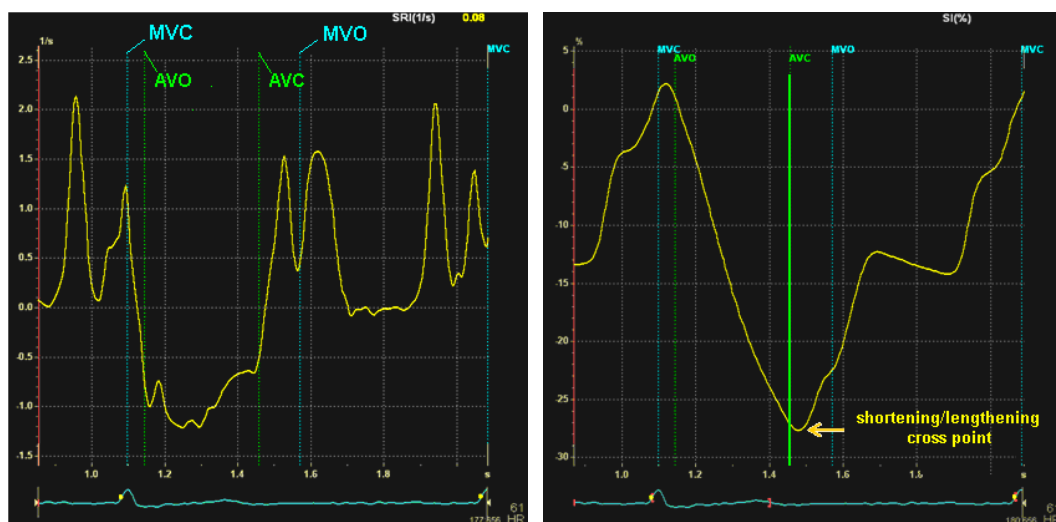
Figure 23: Typical strain rate (above) and strain (below) profiles in a normal subject. There are three peaks from mitral valve closuring (MVC) to mitral valve opening (MVO): the first positive peak lies in isovolumetric contraction time (IVCT), which is narrow and small, the second peak which commonly presents a blunt and large negative peak is during ejection phase, and the following third peak which is similar to the first one is in isovolumetric relaxation time (IVRT). Shortening/lengthening cross point (yellow arrow in the below panel) in strain profile is normally close to the timing of AVC.
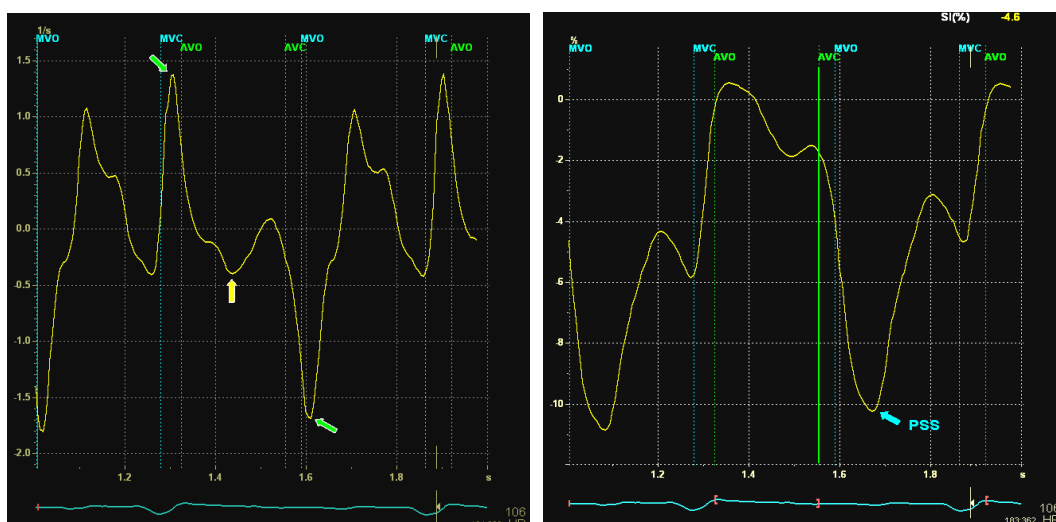
Figure 24: The strain rate and strain profiles in the apical septum of a patient with LVNC. SR_S = - 0.47 1/s, S_max_cyc = - 11.5 %, S_end_sys = - 1.9 %, PSS = 9.6 %. The peak is significantly reduced in ejection phase (yellow arrow in the left panel) with a higher and wider positive peak in IVCT and a larger negative peak in IVRT (green arrow in the left panel). Strain curve shows that shortening/lengthening cross point was delayed until after AVC (blue arrow in the right panel). Effective systolic shortening (end systolic strain) was reduced significantly. SR_S: systolic strain rate during ejection phase; S_end_sys: systolic end strain; PSS: post systolic shortening.

Pathological PSS was measured at apical, mid and basal segment levels of septum and lateral walls in all subjects. As shown in table 5, the overall incidence of pathological PSS was significantly higher in LVNC and DCM group than that in control group (p<0.001). Nevertheless, incidence of PSS was similar between LVNC and DCM group.

Table 5: The incidence of segments with pathological post systolic shortening of septum and lateral wall in control, LVNC and DCM group

	Control (n = 90)		LVNC (n = 78)		DCM (n = 90)	
	Septum	Lateral wall	Septum	Lateral wall	Septum	Lateral wall
Segments, n (%)	6 (13.3)	0	20 (51.3)	15 (38.5)	23 (51.1)	17 (37.8)
Apical, n	5	0	8	4	10	5
Mid, n	0	0	4	5	6	6
Basal, n	1	0	8	6	7	6
Sum, n (%)	6 (6.7)		35 (44.9) *		40 (44.4) *	

* p<0.05 vs. Control

3.5 Strain Rate Imaging Derived from 2D Speckle Tracking

Myocardial deformation in patients with LVNC and DCM was also examined by another novel deformation imaging method (2D speckle tracking imaging). The results were consistent with that demonstrated from TDI method (table 6). Increasing gradient from apex to base was most prominent in lateral wall of LVNC group (figure 25, 26).

Table 6: End systolic strain (S_end_sys) in controls, LVNC and DCM group using 2D speckle tracking imaging

	S_end_sys (%)		
	Control	LVNC	DCM
	n = 15	n = 14	n = 15
Septum			
Apical	- 21.85 ± 3.44	- 5.55 ± 6.55*	- 5.32 ± 5.68*
Mid	- 18.48 ± 3.22	- 6.78 ± 5.30*	- 4.55 ± 5.03*
Basal	- 16.14 ± 4.38‡	- 7.49 ± 4.70*	- 5.90 ± 4.14*
Lateral wall			
Apical	- 20.15 ± 3.25	- 7.01 ± 4.82*	- 6.03 ± 5.23*
Mid	- 20.88 ± 2.33	- 10.2 ± 3.98*	- 6.19 ± 4.24*†
Basal	- 21.69 ± 4.48	- 14.39 ± 4.43*‡§	- 8.84 ± 6.54*†
Inferior wall			
Apical	- 20.94 ± 3.73	- 7.86 ± 6.18*	- 6.55 ± 5.50*
Mid	- 21.39 ± 2.96	- 10.44 ± 5.70*	- 5.70 ± 4.30*†
Basal	- 21.00 ± 3.25	- 13.06 ± 6.64*	- 6.76 ± 4.42*†
Anterior wall			
Apical	- 19.32 ± 4.03	- 5.52 ± 4.65*	- 5.57 ± 5.04*
Mid	- 20.77 ± 2.83	- 8.79 ± 5.36*	- 4.72 ± 4.21*†
Basal	- 18.53 ± 4.13	- 10.71 ± 7.53*	- 6.87 ± 6.42*†
Global average			
Apical	- 20.56 ± 3.65	- 6.49 ± 5.55*	- 5.87 ± 5.25*
Mid	-20.38 ± 3.00	- 9.05 ± 5.20*‡	- 5.29 ± 4.40*†
Basal	- 19.34 ± 4.56	- 11.41 ± 6.38*‡	- 7.09 ± 5.46*†

S_end_sys: end systolic strain

* $p < 0.05$ vs. Control   † $p < 0.05$ vs. LVNC   ‡ $p < 0.05$ vs. Apical   § $p < 0.05$ vs. Mid
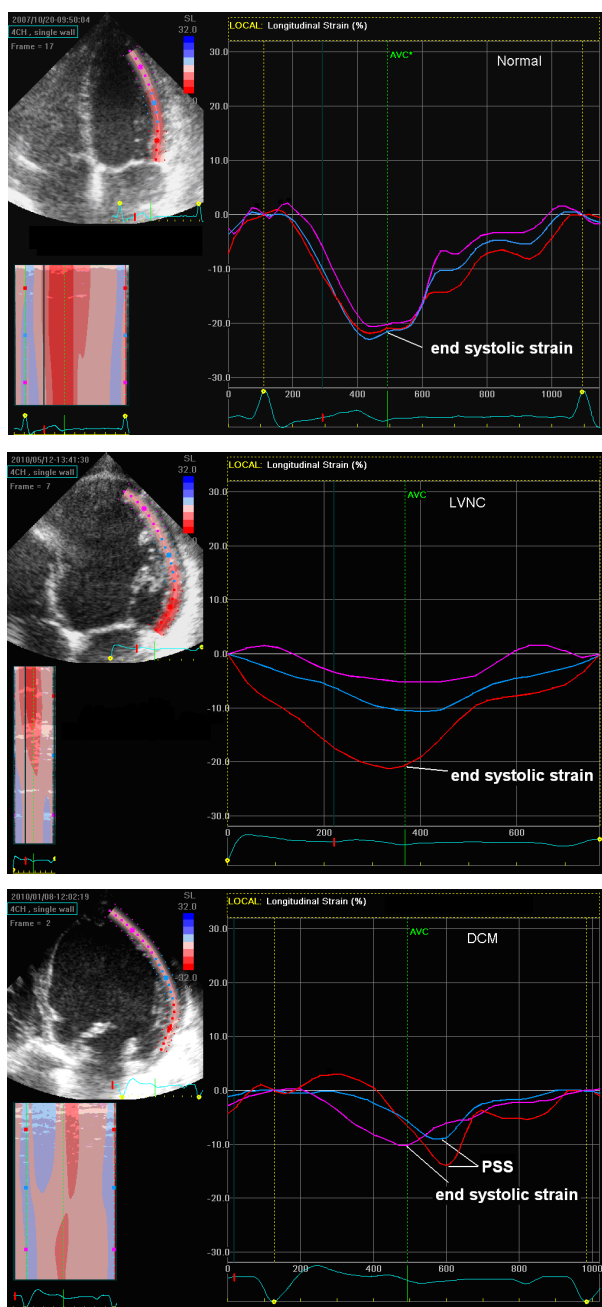
Figure 25: An illustration of strain profiles of lateral walls among control (above), LVNC (middle) and DCM (below) using 2D speckle tracking method. Note a significantly decreased strain in the apical and mid segments (violet and blue curve) compared with a nearly normal strain (red curve) at the basal segment in this LVNC patient. There are no significant differences among apical, mid and basal segments in end systolic strain in the control and DCM patient. Post systolic shortening (PSS) is present in basal and mid lateral wall of the patient with DCM.
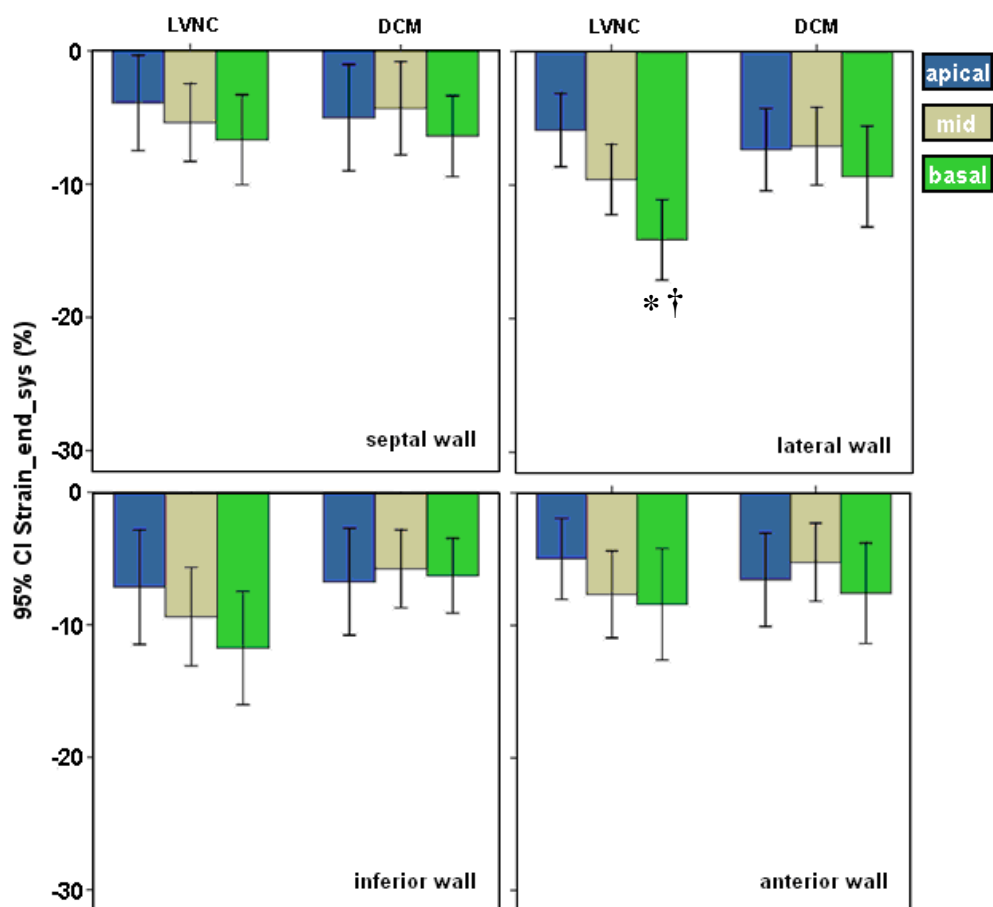
Figure 26: 95% CI end systolic strain by 2D speckle tracking imaging in different walls and different segments between LVNC and DCM group.

* $p<0.05$ vs. apical   † $p<0.05$ vs. mid

3.6 LV Mechanical Asynchrony in LVNC and DCM

3.6.1 Standard Echocardiography

A septal-to-posterior wall motion delay (SPWMD) ≥130ms is a sign of asynchrony of septum and posterior wall contraction[35]. The mean SPWMD was 77 ± 23ms in controls, 126 ± 44ms in LVNC (p<0.01 vs. controls) and 105 ± 44ms in DCM group (p>0.05 vs. controls), respectively. There was no statistical difference between the two patient groups. Incidence of SPWMD ≥ 130ms tended to be higher in patients with LVNC (50%) than in patients with DCM (20%, p=0.191).

The mean of aortic pre-ejection interval (APEI) was 145 ± 30ms in LVNC and 127 ± 33ms in DCM patients, both significantly higher than in controls (87 ± 14ms; all p<0.001). Likewise APEI was similar between the two patient groups. Overall incidence of APEI ≥140ms in patients with LVNC (71.4%) tended to be higher than in patients with DCM 40% (p=0.185).

3.6.2 Tissue Velocity Imaging Results

Tissue velocity-time profiles of four segments (basal and mid septum, basal and mid lateral wall) were measured in all subjects. The time to systolic peak (T_sys) was determined and the time to peak difference in ejection phase between different segments in the same wall as well as in the same segment of different LV walls was calculated (figure 27).

As shown in figure 28, T_sys in all segments of LVNC group was delayed compared to control group (all p<0.05), while in DCM only the two lateral segments were significantly delayed. T_sys in basal lateral, mid lateral and mid-septal segments was similar between the two patient groups (p>0.05), while T_sys in basal septal segments was significantly higher in LVNC group than in DCM group (p<0.05). Moreover, T_sys among various wall segments in the same patient group or control group was similar (p>0.05).
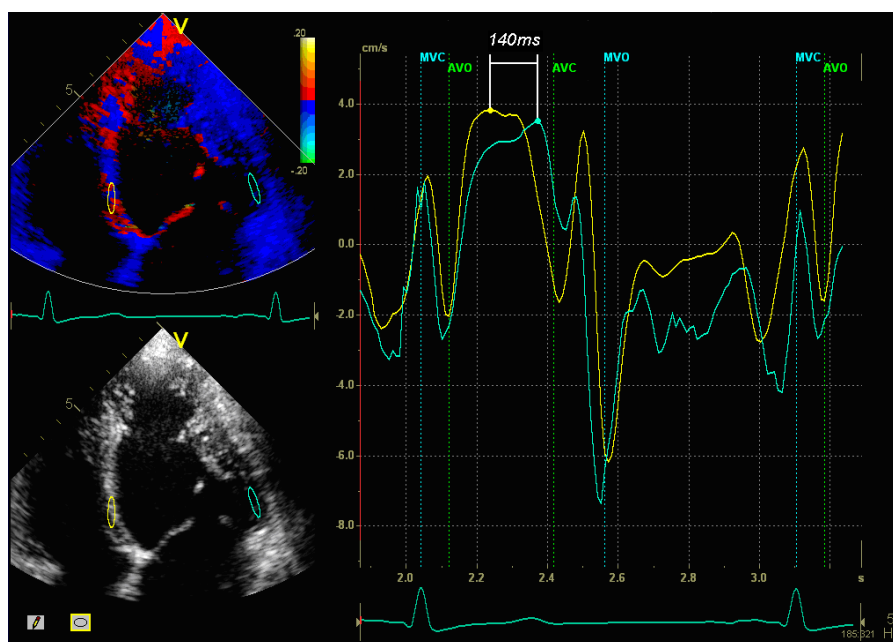
Figure 27: An example of tissue velocity imaging in a patients with LVNC. Regions of interest are respectively at the basal septum (yellow) and basal lateral wall (blue). Note that there is a significant delay in the time to systolic peak (T_sys) of the lateral wall compared with the septum. The difference of time is approximately 140ms.
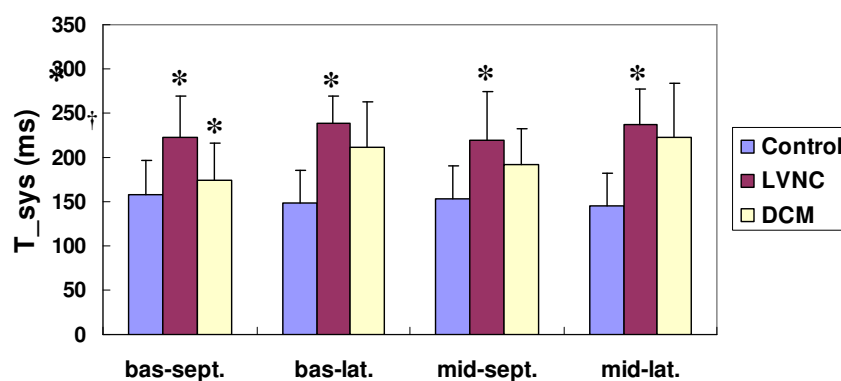
Figure 28: The time to systolic peak (T_sys) during ejection phase in different segments derived by tissue velocity-time profiles.

* $P<0.05$ vs. Control   **†** $p<0.05$ vs. LVNC

3.6.3 Speckle Tracking Results

The time from QRS wave to the compression and expansion crossover (T_{CEC}), which was derived from 2D STI methods, was measured in three segment levels of septum and lateral walls (figure 29). The maximal difference of T_{CEC} (max-Δ T_{CEC}) among six segments was also calculated.

As listed in table 7, the mean T_{CEC} was similar in three segment levels of septum and lateral wall in controls, LVNC and DCM groups. Nevertheless, max-Δ T_{CEC} among six segments in LVNC and DCM group were obviously higher than in the control group (figure 30) and there was no difference on max-Δ T_{CEC} between LVNC and DCM group. In addition, variability of max-Δ T_{CEC} is higher in LVNC and DCM groups (range 67 to 371ms; 86 to 364ms respectively) compared to controls (range 75 to 146ms, figure 30). Further analysis revealed that the time difference between the apical and basal segments of septum and lateral wall (ΔT api-bas) in LVNC group was significantly higher than in controls. This mechanical asynchrony between apical and basal segments was also seen in septum but not in the lateral wall in DCM patients (figure 31).

Table 7: Comparison of the time from QRS wave to the compression and expansion crossover (T_{CEC}, mean ± SD) of three segment levels of septum and lateral wall in control and patient groups

	Control	LVNC	DCM
Septum, n	13	13	15
Apical (ms)	395 ± 48	377 ± 117	398 ± 118
Mid (ms)	377 ± 54	399 ± 112	416 ± 146
Basal (ms)	426 ± 61	382 ± 133	410 ± 136
Lateral wall, n	13	13	15
Apical (ms)	392 ± 49	338 ± 109	359 ± 92
Mid (ms)	382 ± 50	408 ± 70	413 ± 76
Basal (ms)	407 ± 70	444 ± 57	434 ± 80
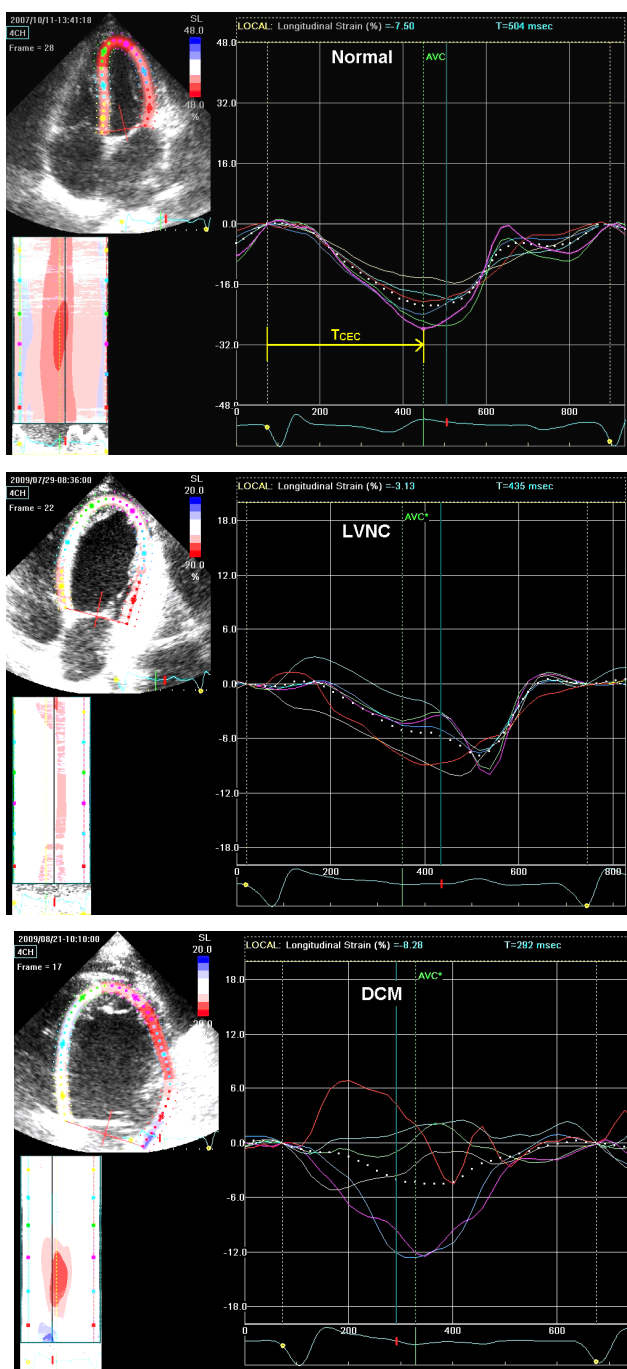
Figure 29: Typical strain profiles derived from 2D speckle tracking imaging in a healthy subject (above) and patients with LVNC (middle) and DCM (below). Note the lack of synchronicity on longitudinal segmental shortening in the LVNC and DCM patient, while T_{CEC} (the time from QRS wave to the compression and expansion crossover) was uniform in control subject.
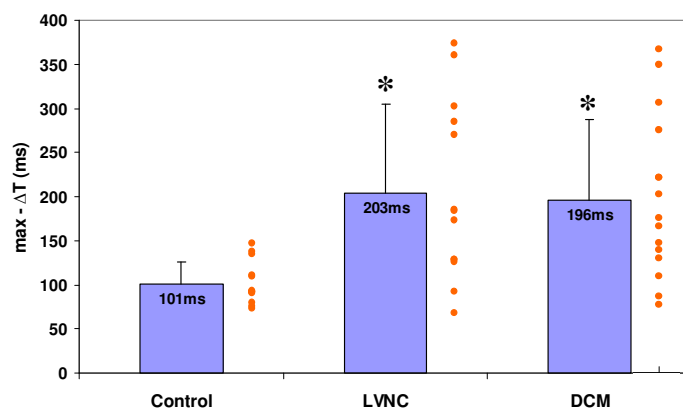
Figure 30: Comparison of the maximal difference of T_{CEC} (mean ± SD) and scatter plot (orange points) in control and patient groups. T_{CEC}: the time from QRS wave to the compression and expansion crossover; max-Δ T_{CEC}: the maximal difference of T_{CEC} among the apical, mid and basal segments of the septum and lateral walls

* $p < 0.05$ vs. Control
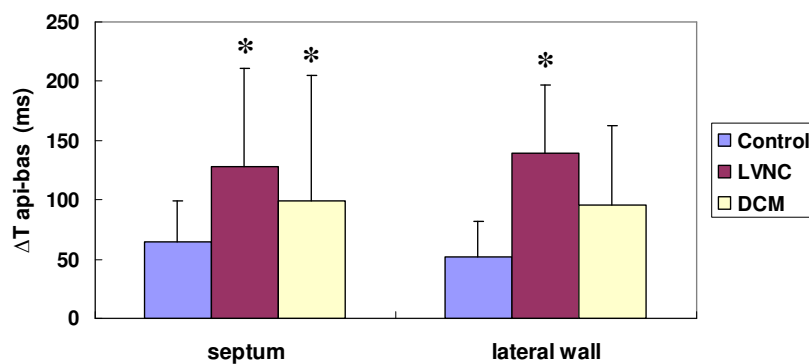
Figure 31: Comparison of the difference of T_{CEC} (mean ± SD) between apical and basal segment of septum and lateral walls in control and patient groups. T_{CEC}: the time from QRS wave to the compression and expansion crossover; ΔT api-bas: the difference of T_{CEC} between the apical and basal segments.

* $p < 0.05$ vs. Control

4. Discussion

This study sought to give a comprehensive description of regional myocardial dysfunction in adult patients with LVNC. The main findings obtained from our patient cohort are:

1. Trabeculations were present in 53.2% segments in patients with LVNC and only in 18.5% segments in patients with DCM. The majority of trabeculations was located in apical and mid segments in both LVNC (99.3%) and DCM patients (92%).

2. Hypertrabeculation (NC/C ratio ≥2.0) was documented in 31.3% segments of LVNC group and only in 3.3% segments of DCM patients and the mean NC/C ratio in LVNC patients was significantly higher than that in DCM patients.

3. The degree of non-compaction was not associated to the global left ventricular systolic function. The regional myocardial shortening (end systolic strain) in non-compacted segments was significantly lower than that in compacted segments. However, there was no linear correlation between non-compaction and end systolic strain.

4. Left and right ventricular regional myocardial systolic deformation was significantly impaired in patients with LVNC and DCM as compared to control subjects. However, a striking difference of regional myocardial systolic function could be seen between LVNC and DCM patients: An increasing myocardial shortening gradient from apex to base was identified in patients with LVNC, whereas DCM displayed a homogeneous reduction of regional function in all segment levels.

5. The increasing myocardial shortening gradient from apex to base was also clearly documented by 2D STI in lateral wall of LVNC patients but not in DCM patients which could serve as a reliable diagnostic sign for differentiating LVNC and DCM.

6. Analysis of myocardial mechanical asynchrony revealed a lack of myocardial contraction synchrony in the LVNC and DCM patients. The time to systolic peak velocity was obviously delayed in these two patient groups and the mechanical asynchrony feature was similar in patients with LVNC and DCM. Moreover both patient groups showed a high incidence of pathological post systolic shortening.

4.1 Morphological Features in LVNC

Isolated left ventricular non-compaction has been recognized as a distinct cardiomyopathy due to its special morphological characteristics. Echocardiography is the most frequently used method to diagnose LVNC.

In our cohort, the non-compacted segments were mainly located at apical and mid segment levels of left ventricle. The entire apical segments of the left ventricle were involved. At mid ventricular level the involved segments were mainly located in left ventricular free wall such as inferior, anterior and posterior wall but not in septum. These results basically correspond to the reports based on echocardiography by Jenni et al. [36], Oechslin et al. [2] and Sengupta et al. [21]. A previous pathological examination confirmed the localization of the non-compacted myocardium corresponding to echocardiographic findings [13]. Left ventricular hypertrabeculation is most frequently described as an abnormal finding of the apex and its adjacent parts of the lateral and inferior wall from pathoanatomic studies, and hypertrabeculation of the interventricular septum was rarely described [7]. Non-compaction was not observed in mid and basal septum in our 14 LVNC patients. In DCM group, there were only 50 segments (18.5%) with trabeculations including 9 with hypertrabeculation, and the majority was located at apical segments. In fact, the mean of NC/C ratio and the number of involved segments were significantly higher in LVNC than that in DCM. Therefore, the differential diagnosis between LVNC and DCM could be easily made based on this remarkable morphological difference of trabeculations by echocardiography in most cases. However, non-compaction is not uniform in LVNC patients and the extent of non-compaction expressed as NC/C ratio ranged from 0.4 to 5.0 and number of involved segments ranged from 2 to 10 in our cohort. The mean of NC/C ratio was greater than 2.1 in 4 out of 14 cases (28.6%), between 1.7 – 2.1 in 7 (50%), and less than 1.7 in 3 cases (21.4%). Although LVNC has been considered as a distinct cardiomyopathy with predominant trabeculations, there is still a subset of cases displaying mild or moderate extent of non-compaction. It is to note that extent of non-compaction with NC/C ratio close to the cut-off value could also be found in DCM, HCM patients and even in healthy individuals. Thus, making the diagnosis just depending on morphological features might be difficult in some cases. Actually, the present proposed diagnostic criteria of LVNC are basically focused on the distinct characteristics of cardiac morphology.

Additionally, a pathological study in a series of 14 cases by Burke et al. described three types of trabeculations: anastomosing broad trabecula, coarse trabecula resembling multiple papillary muscles, and interlacing smaller muscle bundles or relatively smooth endocardial surface with compressed invaginations identified primarily microscopically [37]. The third type could be difficult to be detected by echocardiography due to its gross features. The absence of well-formed papillary muscles could be a complementary sign for the diagnosis. In 5 of 14 patients in our study, a lack of well-formed papillary muscles was identified by echocardiography.

4.2 Extent of Non-compaction and Global LV Function

Our results show that the extent of non-compaction was not associated to the global left ventricular systolic function assessed by ejection fraction in patients with LVNC. Mitral annular displacement, which has recently been considered as a useful indicator to evaluate left ventricular global longitudinal systolic function, was also applied to analyze the correlation between the degree of non-compaction and ventricular performance. In our study, the septal mitral annular displacement in LVNC was significantly lower than the lateral mitral annular displacement despite the fact that the trabeculations were mainly located at the lateral wall but not at the septum. In contrast to previous findings, our results suggest no significant correlation between the extent of non-compaction and the global left ventricular systolic function. Belanger et al. showed in a study of 60 patients a trend towards a negative linear correlation between the NC/C ratio and ejection fraction in their cohort, the similar correlation was found between the LVNC area and ejection fraction [38]. Aras D et al. also suggested age of onset, the total number of affected segments and NC/C ratio could be major determinants of LV systolic dysfunction in patients with LVNC [39]. Lofiego C et al. found that the number of non-compacted segments correlated positively with LV ejection fraction and negatively with LV end-diastolic volume index in the study cohort, and normal wall motion was more common in non-compacted than in compacted segments [40]. Smaller sample size in our study might be one potential reason for failure to document the association between extent of non-compaction and global as well as regional LV dysfunction in patients with LVNC.

The pathophysiologic mechanism of LV systolic dysfunction in LVNC remains unclear. Quantitative evaluation of regional myocardial perfusion performed by positron emission tomography showed a decrease of coronary flow reserve (CFR) in non-compacted segments of the left ventricle despite the absents of coronary circulation abnormalities in patients with LVNC. However, this report showed a decreased CFR was also found in 36 of the 60 segments with non-compaction. Thus, a decreased CFR is not confined to non-compacted segments [41]. Microcirculatory dysfunction probably contributes to left ventricular systolic dysfunction in adults and children with LVNC [41,42].

4.3 Strain Rate Imaging in LVNC

Standard 2D Echocardiography is usually used to observe the cardiac morphological and structural abnormalities and evaluate left ventricular systolic and diastolic function while regional myocardial functional abnormalities could be evaluated by strain rate imaging.

The regional myocardial deformation properties in 252 segments of 14 cases with isolated LVNC were investigated using strain rate imaging derived from TDI and 2D STI in this study. Subsequently, longitudinal deformation of three different segmental levels (basal, mid, apical) was also investigated. Regional myocardial systolic deformation results revealed myocardial impairment at different segment levels (apical, mid, and basal). At apical and mid segment levels, the longitudinal myocardial shortening was significantly reduced, whereas there was only a slightly reduced longitudinal deformation in basal segment level. In fact, some of the LVNC patients even displayed normal or increased systolic deformation at basal segments. Thus, an increasing gradient from apex to base of myocardial systolic function was displayed in the majority of left ventricular walls in patients with LVNC. Of note, this myocardial deformation impairment seemed to be consistent to the distribution of non-compaction, i.e., preserved regional systolic function at the basal segments without pre-existing trabeculations and remarkable regional systolic dysfunction at the non-compacted apical and mid myocardial segments. Moreover, the phenomenon of increasing gradient was more common in lateral, inferior and posterior wall and not common in septum and anteroseptal wall. In fact, trabeculations was also less in septum and anteroseptal wall. Thus, these findings suggest that non-compaction is somehow associated with the regional myocardial deformation impairment in LVNC. Further analysis showed that regional myocardial deformation (the mean of systolic strain rate and end systolic strain) in non-compacted segments (NC/C ratio ≥2.0) was significantly lower than in compacted segments in patients with LVNC. However, no linear correlation was observed between the extent of non-compaction and regional myocardial dysfunction assessed by strain rate imaging, comparable to the non-correlation between global left ventricular function and the extent of non-compaction. These findings might suggest that non-compaction means reduced function, but the severity of reduction can not be deduced by the amount of non-compaction in a segment. Besides trabeculations, regional systolic function might also be affected by regional LV architecture (the thickness and curvature of ventricular walls), local pressure loading, and the basal contraction compensatory mechanism.

4.4 LVNC and DCM

Dilated cardiomyopathy and isolated left ventricular non-compaction often display some similar clinical symptoms and signs as well as echocardiographic findings in a certain subset of patients. Furthermore, it remains unknown whether LVNC is an independent disease or only a kind of morphogenetic abnormality caused by different diseases. There is an ongoing debate if LVNC is a subtype of DCM or not [7,43].

Sengupta et al. reported that patients with LVNC presented with thickened left ventricular walls without enlargement of the ventricular cavity [21]. In our cohort, LV end-diastolic diameter was similarly enlarged in patients with LVNC and DCM. Thus, spherical remodeling was similar between LVNC and DCM group. Obtained deformation information could therefore exclude in some extent the potential effect derived from ventricular spherical remodeling.

Tufekcioglu O et al. compared the differences between LVNC and DCM by systolic myocardial velocities along the long axis and short axis derived from pulsed Doppler tissue imaging. They found that patients with LVNC and DCM showed similar velocity properties along the long axis and short axis of the LV [22]. However, it has to be mentioned that myocardial Doppler velocity imaging cannot differentiate active contraction from passive motion as a result of tethering of adjacent segments or global heart motion [24] Deformation imaging could get rid of this limitation and could reflect regional myocardial shortening/lengthening or thickening/thinning without the influence of segments interaction. Vicario et al. suggested peak systolic strain rate appears to be more useful than TDI velocities on evaluating left ventricular dynamics during volume loading in patients with depressed left ventricular function. Different from tissue Doppler velocities, segmental strain describes the regional myocardial deformation which is related to local myocardial contractility changes [44]. Curved M-mode strain rate imaging was reported by Williams RI et al. in a single LVNC case, and revealed uncoordinated myocardial contraction in this LVNC patient. In our cohort, Doppler-derived strain rate and strain were used to investigate the more subtle differences in regional myocardial function between patients with LVNC and DCM. Even though remarkably regional myocardial dysfunction was documented in both patients with LVNC and DCM, the regional myocardial deformation impairment properties were strikingly different between the two patient groups. Regional myocardial dysfunction in patients with DCM displayed a homogeneous regional myocardial deformation reduction in all segment levels, while regional myocardial function analysis displayed the described uneven impairment with the increasing shortening grading from apex to the base in patients with LVNC. Thus, this gradient might be a useful echocardiographic marker to differentiate LVNC from DCM. However, further studies are warranted to see if the increased gradient from apex to base is a distinct hallmark for LVNC or just a non-specific feature possibly also displayed in other disorders with heart failure and LV remodeling.

4.5 Tissue Doppler Imaging and 2D Speckle Tracking Imaging

2D speckle tracking imaging is a promising echocardiographic technology based on tissue tracking from two dimensional grey scale images. Segmental myocardial function can be analyzed

quantitatively by 2D speckle tracking imaging; less angel dependency is the major advantage of 2D speckle tracking imaging compared to TDI technique. It has been proposed to apply 2D STI to clinical echo measurements rather than TDI in virtue of more rapid tracking, parameter extraction as well as automatic segmentation [45-47]. In clinical practice, tissue Doppler imaging is generally perceived to be more difficult to master in post processing. The reproducibility of speckle tracking imaging of LV seems to be generally better than that of tissue Doppler [47].

The results of 2D STI in our cohort were generally consistent with those of Doppler-derived strain rate imaging and the typical gradient in LVNC could also be easily reproduced by 2D STI. Actually, the strain and strain rate profiles of three segments by 2D speckle tracking can be quickly displayed simultaneously. This modality is more intuitive for observing regional myocardial deformation gradient changes in different segment levels. Furthermore, we compared the post-processing time between TDI method and 2D speckle tracking imaging. The mean post-processing time of TDI analysis for 18 segments of six LV walls in control group was approximately 32 minutes while that of 2D speckle tracking 9 minutes. The intra-observer agreement of measurements also showed that 2D STI is superior to TDI (coefficient of reproducibility in strain rate: 0.87 vs. 0.71; strain: 0.94 vs. 0.83). Automatic segmentation of 2D speckle tracking can give a better repeatability than manual placement of the ROI and this may be a reason why 2D speckle tracking method present better reproducibility than TDI method. However, Modesto et al. found a much better correspondence between TDI and 2D strain, with correlations of 0.94 and 0.96 for strain rate and strain respectively [48].

4.6 Features of Strain and Strain Rate Profiles in LVNC

The shape of the strain or strain rate curve is another important feature to demonstrate the regional myocardial deformation properties besides quantitative peak values. No studies are available describing the shape features of the strain and strain rate curves in patients with LVNC. As compared to the control group, pathological post systolic shortening (PSS) was more common in patients with LVNC as well as in DCM in this study, with no significant difference between the two patient groups.

Post systolic shortening reflects a delayed myocardial contraction occurring after the aortic valve closure. PSS has been described in experimental and clinical studies. PSS probably results from a passive inward movement caused by adjacent normal contracting myocardial segments and seems to be associated with myocardial bulging or elastic recoil [49]. Another explanation for PSS is the muscle tension prolongation which represents a delayed active contraction appearing after LV segment unloading and regional wall stress reduction [50]. Therefore, PSS appears to be a marker of myocardial

ischemia and also may occur in non-ischemic cardiac diseases with left ventricular hypertrophy and volume overload, and left bundle branch block. PSS in LVNC patient might reflect ischemic myocardium or fibrotic myocardium or both [34,41,42,51,52].

It is of importance to evaluate changes of strain rate curve occurring during IVCT in combination with systolic peak values during ejection phase and post systolic shortening occurring during IVRT in dyskinetic myocardium. In general, LV pressure peaks during IVCT and falls during IVRT steeply. However, dyskinetic myocardium lengthens at the time of LV pressure rising and shortens at the time of LV pressure falling [49]. This phenomenon can be demonstrated by strain rate imaging (figure 24). This characteristic profile seems to be quite common in the septum of patients with LVNC while the incidence of this characteristic profile was similar in apical and basal segments of various LV walls. Future studies are needed to verify if this phenomenon is a specific or nonspecific hallmark of patients with LVNC [51-53].

4.7 LV Mechanical Asynchrony in LVNC

In this study, standard 2D echocardiography, tissue velocity imaging and strain rate imaging were used to evaluate myocardial mechanical asynchrony in LVNC. The underlying mechanism of asynchrony in LVNC seems to be linked with chronic heart failure and left bundle branch block. The relevant pathological characteristics include specific morphological abnormality (myocardial non-compaction), subendocardial and interstitial fibrosis, microcirculatory dysfunction and left ventricular spherical remodeling [8-14,41,42].

SPWMD was significantly prolonged in patients with LVNC compared with control group (126ms vs. 77ms). Since SPWMD is merely an observation of the septum and posterior wall synchrony, it thus cannot represent the variation of the entire cardiac contraction synchrony/asynchrony. Likewise, the mean of APEI of both patient groups was equally delayed as compared to control group.

Velocity differences of segmental myocardium could be readily evaluated on tissue velocity curves derived from TDI. Intraventricular mechanical asynchrony could be reflected by calculating the time from onset of QRS to peak velocity during ejection phase (T_sys). A significant delay in T_sys could be observed in patients with LVNC in our cohort. Different from the report of Schuster et al. [54], the delay between septum and lateral wall based on TVI method was not found in LVNC and DCM groups in the present study.

Yu CM et al. showed that tissue Doppler imaging is superior to strain rate imaging on predicting reverse remodeling after cardiac resynchronization therapy [55]. Paradoxical alternation bands of

compression and expansion throughout systole and diastole in non-compacted lateral wall using curved M-mode (C-mode) strain rate profile was recorded by Williams RI et al., suggesting an in-coordinated myocardial contraction in patients with LVNC [56]. We investigated the myocardial asynchrony using deformation imaging derived from 2D speckle tracking. Though mean T_{CEC} was similar among different segment levels, the maximal time to peak (max-Δ T_{CEC}) between apical and basal segments revealed remarkably systolic asynchrony in patients with LVNC. As demonstrated in figure 29, myocardial contraction asynchrony among different segments could be clearly demonstrated by strain profiles. Recently, improvement of the novel imaging modalities such as Real-time 3D echocardiography has overcome certain limitations and might enable evaluation of mechanical asynchrony more easily.

It appears that mechanical asynchrony is a common phenomenon in LVNC patients complicating heart failure. LV mechanical asynchrony evaluation is needed in clinical setting to predict the response of cardiac resynchronization therapy (CRT). Our study suggests that conventional and TDI technique as well as SRI could be useful tools to detect the mechanical asynchrony in patients with LVNC.

4.8 Clinical Implications

In this study, the regional myocardial systolic dysfunction of patients with LVNC was comprehensively investigated by several echocardiographic modalities. An uneven impairment in different segmental levels of LVNC was revealed for the first time. An increasing shortening gradient from apex to base was demonstrated by two novel deformation imaging modalities. This striking feature might be useful to differentiate patients with LVNC and DCM. For the clinicians, it is easy to establish the diagnosis of left ventricular non-compaction using conventional echocardiography or cardiac MRI depending on the distinct non-compacted cardiac architecture with the triad of heart failure, arrhythmias and embolic events in some cases. However, it might be a challenge to distinguish LVNC from DCM when patients only display mild or moderate degree of non-compaction. In this case, 2D speckle tracking imaging could provide complementary information on the subtle differences in regional myocardial deformation for differential diagnosis. Moreover, this technique is practical because it is easy to perform and the post processing analysis is not time-consuming. Besides differential diagnosis, it might also be an effective hallmark for monitoring the disease progression and therapy effectiveness. Of cause, this assumption needs to be confirmed by further follow-up studies. As for strain rate imaging derived from TDI and 2D speckle tracking, the two methods present similar value in quantitative analysis of regional myocardial impairment. However, it is important to be aware

of the limitations of individual method. As a result of the nature of Doppler-derived strain rate, it is generally perceived as more difficult to master in post processing in clinical practice. 2D STI is potentially more applicable on accessing regional myocardial function in clinical settings based on clinical and experimental research results. On the whole, both 2D speckle tracking imaging and TDI are of equal or complementary value in the quantitative analysis of regional myocardial function in patients with LVNC.

4.9 Limitations

This study comprised a relatively small number of subjects, thus potential selection bias of patients could not be avoided. Further studies with larger cohorts are needed to confirm the findings. We focused on the features of regional myocardial function in patients with LVNC using different echocardiographic modalities in this study. However, the underlying substantial mechanism of these findings remains unclear. This study mainly analyzed systolic myocardial deformation, while the diastolic deformation was not analyzed.

5. Conclusion

Patients with isolated left ventricular non-compaction show typical morphological presentation and a diagnosis could often be made based on standard 2D echocardiography. However, an increasing shortening gradient from apex to base illustrated through TDI and 2D speckle tracking has potential diagnostic value for differentiating patients with LVNC and DCM. Both 2D STI and TDI are of equal or complementary value in the quantitative analysis of regional myocardial function.

6. Acknowledgements

I would like to express my gratitude to all those who helped me during my staying in Wuerzburg for thesis work.

My deepest gratitude goes first and foremost to Professor Dr. Frank Weidemann, my supervisor. I thank him for his respect, his tolerance, his thoughtfulness, and the many opportunities he gave me to be a part of a rigorous cardiological research team. I thank him for the thoughtful discussions which guide me during my work in this team and stimulate my growing interest in this area of research. The thesis work would not have been finished without his consistent and illuminating instruction.

My deepest gratitude goes also to Professor Dr. Georg Ertl for the opportunity to work in this wonderful clinic.

I would like to thank Dr. Markus Niemann for his generous help and he solved all problems I encountered during my stay here.

I would like to thank Dr. Kai Hu, his suggestions made my work and living here more enjoyable. I also thank him for helping me on the thesis writing.

I'd like to thank Dr. Sebastian Herrmann, Phillipp Gaudron, Julia Afanasjew, for their time, support, and effort to help me in all respects.

Finally, my thanks would go to my beloved family for their loving considerations, great confidence and support all through these years.

7. References

1. Engberding R, Bender F. Identification of a rare congenital anomaly of the myocardium by two-dimensional echocardiography: persistence of isolated myocardial sinusoids. *Am J Cardiol.* 1984;53:1733-4.c

2. Oechslin EN, Attenhofer Jost CH, Rojas JR, Kaufmann PA, Jenni R. Long-term follow-up of 34 adults with isolated left ventricular noncompaction: a distinct cardiomyopathy with poor prognosis. *J Am Coll Cardiol.* 2000;36:493-500.

3. Stöllberger C, Finsterer J, Blazek G. Isolated left ventricular abnormal trabeculation is a cardiac manifestation of neuromuscular disorders. *Cardiology.* 2000;94:72-6.

4. Stöllberger C, Finsterer J, Blazek G. Left ventricular hypertrabeculation/noncompaction and association with additional cardiac abnormalities and neuromusculzar disorders. *Am J Cardiol.* 2002;90:899-902.

5. Ritter M, Oechslin E, Sütsch G, Attenhofer C, Schneider J, Jenni R. Isolated noncompaction of the myocardium in adults. *Mayo Clin Proc.* 1997;72:26-31.

6. Ichida F, Tsubata S, Bowles KR, Haneda N, Uese K, Miyawaki T, Dreyer WJ, Messina J, Li H, Bowles NE, Towbin JA. Novel gene mutations in patients with left ventricular noncompaction or Barth syndrome. *Circulation.* 2001;103:1256-63.

7. Stöllberger C, Finsterer J. Left ventricular hypertrabeculation/noncompaction. *J Am Soc Echocardiogr.* 2004;17:91-100.

8. Chin TK, Perloff JK, Williams RG, Jue K, Mohrmann R. Isolated noncompaction of left ventricular myocardium. A study of eight cases. *Circulation.* 1990;82:507-13.

9. Allenby PA, Gould NS, Schwartz MF, Chiemmongkoltip P.Dysplastic cardiac development presenting as cardiomyopathy. *Arch Pathol Lab Med.* 1988;112:1255-8.

10. Bleyl SB, Mumford BR, Brown-Harrison MC, Pagotto LT, Carey JC, Pysher TJ, Ward K, Chin TK. Xq28-linked noncompaction of the left ventricular myocardium: prenatal diagnosis and pathologic analysis of affected individuals. *Am J Med Genet.* 1997;72:257-65.

11. Dusek J, Ostádal B, Duskova M. Postnatal persistence of spongy myocardium with embryonic blood supply. *Arch Pathol.* 1975;99:312-7.

12. Rose AG. Multiple coronary arterioventricular fistulae. *Circulation.* 1978;58:178-80.

13. Jenni R, Oechslin E, Schneider J, Attenhofer Jost C, Kaufmann PA. Echocardiographic and pathoanatomical characteristics of isolated left ventricular non-compaction: a step towards classification as a distinct cardiomyopathy. *Heart.* 2001;86:666-71.

14. Neudorf UE, Hussein A, Trowitzsch E, Schmaltz AA. Clinical features of isolated noncompaction of the myocardium in children. *Cardiol Young.* 2001;11:439-42.

15. Amann G, Sherman FS. Myocardial dysgenesis with persistent sinusoids in a neonate with Noonan's phenotype. *Pediatr Pathol.* 1992;12:83-92.

16. Kurosaki K, Ikeda U, Hojo Y, Fujikawa H, Katsuki T, Shimada K. Familial isolated noncompaction of the left ventricular myocardium. *Cardiology.* 1999;91:69-72.

17. Ichida F, Hamamichi Y, Miyawaki T, Ono Y, Kamiya T, Akagi T, Hamada H, Hirose O, Isobe T, Yamada K, Kurotobi S, Mito H, Miyake T, Murakami Y, Nishi T, Shinohara M, Seguchi M, Tashiro S, Tomimatsu H. Clinical

features of isolated noncompaction of the ventricular myocardium: long-term clinical course, hemodynamic properties, and genetic background. *J Am Coll Cardiol.* 1999;34:233-40.

18. Stöllberger C, Finsterer J, Blazek G. Isolated left ventricular abnormal trabeculation: follow-up and association with neuromuscular disorders. *Can J Cardiol.* 2001;17:163-8.

19. Murphy RT, Thaman R, Blanes JG, Ward D, Sevdalis E, Papra E, Kiotsekoglou A, Tome MT, Pellerin D, McKenna WJ, Elliott PM. Natural history and familial characteristics of isolated left ventricular non-compaction. *Eur Heart J.* 2005;26:187-92.

20. Boyd MT, Seward JB, Tajik AJ, Edwards WD. Frequency and location of prominent left ventricular trabeculations at autopsy in 474 normal human hearts: implications for evaluation of mural thrombi by two-dimensional echocardiography. *J Am Coll Cardiol.* 1987;9:323-6.

21. Sengupta PP, Mohan JC, Mehta V, Jain V, Arora R, Pandian NG, Khandheria BK. Comparison of echocardiographic features of noncompaction of the left ventricle in adults versus idiopathic dilated cardiomyopathy in adults. *Am J Cardiol.* 2004;94:389-91.

22. Tufekcioglu O, Aras D, Ozeke O, Maden O, Topaloglu S. Comparison of regional systolic myocardial velocities in patients with isolated left ventricular noncompaction and patients with idiopathic dilated cardiomyopathy. *J Am Soc Echocardiogr.* 2006;19:1320-5.

23. Vatta M, Mohapatra B, Jimenez S, Sanchez X, Faulkner G, Perles Z, Sinagra G, Lin JH, Vu TM, Zhou Q, Bowles KR, Di Lenarda A, Schimmenti L, Fox M, Chrisco MA, Murphy RT, McKenna W, Elliott P, Bowles NE, Chen J, Valle G, Towbin JA. Mutations in Cypher/ZASP in patients with dilated cardiomyopathy and left ventricular non-compaction. *J Am Coll Cardiol.* 2003;42:2014-27.

24. Urheim S, Edvardsen T, Torp H, Angelsen B, Smiseth OA. Myocardial strain by Doppler echocardiography. Validation of a new method to quantify regional myocardial function. *Circulation.* 2000;102:1158-64.

25. Kowalski M, Kukulski T, Jamal F, D'hooge J, Weidemann F, Rademakers F, Bijnens B, Hatle L, Sutherland GR. Can natural strain and strain rate quantify regional myocardial deformation? A study in healthy subjects. *Ultrasound Med Biol.* 2001;27:1087-97.

26. Dalen H, Thorstensen A, Aase SA, Ingul CB, Torp H, Vatten LJ, Stoylen A. Segmental and global longitudinal strain and strain rate based on echocardiography of 1266 healthy individuals: the HUNT study in Norway. *Eur J Echocardiogr.* 2010;11:176-83.

27. Nesbitt GC, Mankad S, Oh JK. Strain imaging in echocardiography: methods and clinical applications. *Int J Cardiovasc Imaging.* 2009;25:9-22.

28. Nesbitt GC, Mankad S. Strain and strain rate imaging in cardiomyopathy. *Echocardiography.* 2009;26:337-44.

29. Weidemann F, Jung P, Hoyer C, Broscheit J, Voelker W, Ertl G, Störk S, Angermann CE, Strotmann JM. Assessment of the contractile reserve in patients with intermediate coronary lesions: a strain rate imaging study validated by invasive myocardial fractional flow reserve. *Eur Heart J.* 2007;28:1425-32.

30. Weidemann F, Dommke C, Bijnens B, Claus P, D'hooge J, Mertens P, Verbeken E, Maes A, Van de Werf F, De Scheerder I, Sutherland GR. Defining the transmurality of a chronic myocardial infarction by ultrasonic strain-rate imaging: implications for identifying intramural viability: an experimental study. *Circulation.* 2003;107:883-8.

31. Weidemann F, Jamal F, Sutherland GR, Claus P, Kowalski M, Hatle L, De Scheerder I, Bijnens B, Rademakers FE. Myocardial function defined by strain rate and strain during alterations in inotropic states and heart rate. *Am J Physiol Heart Circ Physiol.* 2002;283:H792-9.

32. Weidemann F, Eyskens B, Sutherland GR. New ultrasound methods to quantify regional myocardial function in children with heart disease. *Pediatr Cardiol.* 2002;23:292-306.

33. Jamal F, Strotmann J, Weidemann F, Kukulski T, D'hooge J, Bijnens B, Van de Werf F, De Scheerder I, Sutherland GR. Noninvasive quantification of the contractile reserve of stunned myocardium by ultrasonic strain rate and strain. *Circulation.* 2001;104:1059-65.

34. Voigt JU, Lindenmeier G, Exner B, Regenfus M, Werner D, Reulbach U, Nixdorff U, Flachskampf FA, Daniel WG. Incidence and characteristics of segmental postsystolic longitudinal shortening in normal, acutely ischemic, and scarred myocardium. *J Am Soc Echocardiogr.* 2003;16:415-23.

35. Pitzalis MV, Iacoviello M, Romito R, Guida P, De Tommasi E, Luzzi G, Anaclerio M, Forleo C, Rizzon P. Ventricular asynchrony predicts a better outcome in patients with chronic heart failure receiving cardiac resynchronization therapy. *J Am Coll Cardiol.* 2005;45:65-9.

36. Jenni R, Oechslin EN, van der Loo B. Isolated ventricular non-compaction of the myocardium in adults. *Heart.* 2007;93:11-5.

37. Burke A, Mont E, Kutys R, Virmani R. Left ventricular noncompaction: a pathological study of 14 cases. *Hum Pathol.* 2005;36:403-11.

38. Belanger AR, Miller MA, Donthireddi UR, Najovits AJ, Goldman ME. New classification scheme of left ventricular noncompaction and correlation with ventricular performance. *Am J Cardiol.* 2008;102:92-6.

39. Aras D, Tufekcioglu O, Ergun K, Ozeke O, Yildiz A, Topaloglu S, Deveci B, Sahin O, Kisacik HL, Korkmaz S. Clinical features of isolated ventricular noncompaction in adults long-term clinical course, echocardiographic properties, and predictors of left ventricular failure. *J Card Fail.* 2006;12:726-33.

40. Lofiego C, Biagini E, Ferlito M, Pasquale F, Rocchi G, Perugini E, Leone O, Bracchetti G, Caliskan K, Branzi A, ten Cate FJ, Rapezzi C. Paradoxical contributions of non-compacted and compacted segments to global left ventricular dysfunction in isolated left ventricular noncompaction. *Am J Cardiol.* 2006;97:738-41.

41. Jenni R, Wyss CA, Oechslin EN, Kaufmann PA. Isolated ventricular noncompaction is associated with coronary microcirculatory dysfunction. *J Am Coll Cardiol.* 2002;39:450-4.

42. Junga G, Kneifel S, Von Smekal A, Steinert H, Bauersfeld U. Myocardial ischaemia in children with isolated ventricular non-compaction. *Eur Heart J.* 1999;20:910-6.

43. Biagini E, Ragni L, Ferlito M, Pasquale F, Lofiego C, Leone O, Rocchi G, Perugini E, Zagnoni S, Branzi A, Picchio FM, Rapezzi C. Different types of cardiomyopathy associated with isolated ventricular noncompaction. *Am J Cardiol.* 2006;98:821-4.

44. Vicario ML, Caso P, Martiniello AR, Fontanella L, Petretta M, Sardu C, Petretta MP, Bonaduce D. Effects of volume loading on strain rate and tissue Doppler velocity imaging in patients with idiopathic dilated cardiomyopathy. *J Cardiovasc Med (Hagerstown).* 2006;7:852-8.

45. Artis NJ, Oxborough DL, Williams G, Pepper CB, Tan LB. Two-dimensional strain imaging: a new echocardiographic advance with research and clinical applications. *Int J Cardiol.* 2008;123:240-8.

46. Perk G, Tunick PA, Kronzon I. Non-Doppler two-dimensional strain imaging by echocardiography--from technical considerations to clinical applications. *J Am Soc Echocardiogr.* 2007;20:234-43.

47. Teske AJ, De Boeck BW, Melman PG, Sieswerda GT, Doevendans PA, Cramer MJ. Echocardiographic quantification of myocardial function using tissue deformation imaging, a guide to image acquisition and analysis using tissue Doppler and speckle tracking. Cardiovasc *Ultrasound.* 2007;5:27.

48. Modesto KM, Cauduro S, Dispenzieri A, Khandheria B, Belohlavek M, Lysyansky P, Friedman Z, Gertz M, Abraham TP.Two-dimensional acoustic pattern derived strain parameters closely correlate with one-dimensional tissue Doppler derived strain measurements. *Eur J Echocardiogr.* 2006;7:315-21.

49. Skulstad H, Edvardsen T, Urheim S, Rabben SI, Stugaard M, Lyseggen E, Ihlen H, Smiseth OA. Postsystolic shortening in ischemic myocardium: active contraction or passive recoil? *Circulation.* 2002;106:718-24.

50. Takayama M, Norris RM, Brown MA, Armiger LC, Rivers JT, White HD. Postsystolic shortening of acutely ischemic canine myocardium predicts early and late recovery of function after coronary artery reperfusion. *Circulation.* 1988;78:994-1007.

51. Claus P, Weidemann F, Dommke C, Bito V, Heinzel FR, D'hooge J, Sipido KR, Sutherland GR, Bijnens B. Mechanisms of postsystolic thickening in ischemic myocardium: mathematical modelling and comparison with experimental ischemic substrates. *Ultrasound Med Biol.* 2007;33:1963-70.

52. Song JM, Kim JH, Kim YH, Lee SW, Yoon YJ, Kim J, Kang DH, Song JK. Temporal changes and histologic relation of postsystolic thickening in an animal model of acute ischemia and reperfusion. *J Am Soc Echocardiogr.* 2003;16:409-14.

53. Weidemann F, Broscheit JA, Bijnens B, Claus P, Sutherland GR, Voelker W, Ertl G, Strotmann JM. How to distinguish between ischemic and nonischemic postsystolic thickening: a strain rate imaging study. *Ultrasound Med Biol.* 2006;32:53-9.

54. Schuster P, Faerestrand S, Ohm OJ. Color Doppler tissue velocity imaging demonstrates significant asynchronous regional left ventricular contraction and relaxation in patients with bundle branch block and heart failure compared with control subjects. *Cardiology.* 2004;102:220-7.

55. Yu CM, Fung JW, Zhang Q, Chan CK, Chan YS, Lin H, Kum LC, Kong SL, Zhang Y, Sanderson JE. Tissue Doppler imaging is superior to strain rate imaging and postsystolic shortening on the prediction of reverse remodeling in both ischemic and nonischemic heart failure after cardiac resynchronization therapy. *Circulation.* 2004;110:66-73.

56. Williams RI, Masani ND, Buchalter MB, Fraser AG. Abnormal myocardial strain rate in noncompaction of the left ventricle. *J Am Soc Echocardiogr.* 2003;16:293-6.

Curriculum Vitae

Family Name: Liu

Given Name: Dan

Gender: Female

Date of Birth: 09-16-1975

Citizenship：Chinese

Place of Birth: Wuhan, Hubei Province, China

Major: Cardiology, Internal medicine

E-mail: E_Liu_D@medizin.uni-wuerzburg.de

       danliu32@googlemail.com

Address: Medizinische Klinik und Poliklinik I

Universitaetsklinik Wuerzburg

Oberduerrbacher Str.6

97080 Wuerzburg

Tel: 0049 931 20139710

       0049 163 9062872

EDUCATION

September 1993 - July 1998

Bachelor of Clinical Medicine, Medical College of Wuhan University

September 2002 - July 2006

Master of Internal Medicine, Medical College of Wuhan University

March 2009 - Present

Doctoral degree student, University Würzburg

PRACTICAL EXPERIENCES

October 1999 - October 2008

Sonographer in the Wuhan Commercial Hospital, Hubei Province, China

July 2005 - October 2008

Attending physician and the deputy director in Ultrasound Department of Wuhan Commercial Hospital

February 2007 - May 2007

Training for 3D-Ultrasound in Wujingzongdui Hospital, Wuhan, Hubei Province

December 2008- February 2009

Training for echocardiography in Wuhan Asia Heart Hospital, Hubei Province

RESEARCH EXPERIENCES

2004~2005

Value of ultrasound on predicting the fetal intrauterine anoxia in late pregnancy

Value of 2D ultrasound imaging and Color Doppler Flow Imaging on patients with Hashimoto's
Thyroiditis

2005~2006 (M.Sc.)

Value of Color Doppler Flow Imaging on monitoring the lesion of micro-vessel (central retinal artery)
in hypertensive pregnancy

EXPERIMENTAL SKILLS

2D-Ultrasound

Color Doppler Flow Imaging

Echocardiography

3D-Ultrasound

ECG

Holter

PUBLICATIONS

1. Dan Liu, Ruiqiang Guo, Keli Zhou, et al. Study the Method of All-Round Evaluation on Prediction of the Fetal Intrauterine Anoxia in Late Pregnancy. J New Med 2006;16:32

2. Dan Liu, Keli Zhou, Weining Liu. Clinical Analysis of B-Ultrasound in Diagnosis of the Early Pregnancy. Central China Med J. 2004;28:332

3. Dan Liu, Ruiqiang Guo, Keli Zhou. The Value of B-Ultrasound Imaging and Color Doppler Flow Imaging in Hashimoto's thyroiditis. J Mathematical Med. 2006;19:147

4. Dan Liu, Keli Zhou, Weining Liu, et al. Clinical Value of ECG Diagnosis Criteria for Left Atrial Amplification. J New Med. 2004;14:170